Phase, composition and growth mechanism for secondary organic aerosol from the ozonolysis of α-cedrene

Y. Zhao, L. M. Wingen, V. Perraud, and B. J. Finlayson-Pitts*

Department of Chemistry
University of California
Irvine, CA 92697, USA

*Corresponding author: Email: bjfinlay@uci.edu; phone: (949) 824-7670; Fax: (949) 824-2420

cedrene_SOA_text_final_021516.doc

Abstract

Sesquiterpenes are an important class of biogenic volatile organic compounds (BVOCs) and have a high secondary organic aerosol (SOA) forming potential. However, SOA formation from sesquiterpene oxidation has received less attention compared to other BVOCs such as monoterpenes, and the underlying mechanisms remain poorly understood. In this work, we present a comprehensive experimental investigation of the ozonolysis of α-cedrene both in a glass flow reactor (27-44 s reaction times) and in static Teflon chambers (30-60 min reaction times). The SOA was collected by impaction or filters, followed by analysis using attenuated total reflectance-Fourier transform infrared spectroscopy (ATR-FTIR) and electrospray ionization mass spectrometry (ESI-MS), or measured on line using direct analysis in real time (DART-MS) and aerosol mass spectrometry (AMS). The slow evaporation of 2-ethylhexyl nitrate that was incorporated into the SOA during its formation and growth gives an estimated diffusion coefficient of 3×10^{-15} cm^2 s^{-1} and shows that SOA is a highly viscous semi-solid. Possible structures of four newly observed low molecular weight (MW ≤ 300 Da) reaction products with higher oxygen content than those previously reported were identified. High molecular weight (HMW) products formed in the early stages of the oxidation have structures consistent with aldol condensation products, peroxyhemiacetals, and esters. The size-dependent distributions of HMW products in the SOA, as well as the effects of stabilized Criegee intermediate (SCI) scavengers on HMW products and particle formation, confirm that HMW products and reactions of Criegee intermediates play a crucial role in early stages of particle formation. Our studies provide new insights into mechanisms of SOA formation and growth in α-cedrene ozonolysis and the important role of sesquiterpenes in new particle formation as suggested by field measurements.

1. Introduction

Organic aerosol is ubiquitous in the atmosphere and has an important influence on air quality (Finlayson-Pitts and Pitts, 2000; Seinfeld and Pandis, 2006; Zhang et al., 2015), climate (Kanakidou et al., 2005; IPCC, 2013), and human health (Mauderly and Chow, 2008; Shiraiwa et al., 2012). Secondary organic aerosol (SOA) formed from the oxidation of volatile organic compounds (VOCs) contributes a substantial fraction (up to 90%) of organic aerosol (Zhang et al., 2007). Biogenic VOCs (BVOCs) such as isoprene (C_5H_8), monoterpenes ($C_{10}H_{16}$), and sesquiterpenes ($C_{15}H_{24}$) account for ~ 90% of global VOC emissions (Guenther et al., 1995; Goldstein and Galbally, 2007) and are the dominant contributors to global SOA formation upon reaction with oxidants that are mainly anthropogenically derived (Kanakidou et al., 2005; Hallquist et al., 2009).

Sesquiterpenes are an important class of BVOCs, with emissions being estimated as 9-29% of those of monoterpenes (Helmig et al., 2007; Sakulyanontvittaya et al., 2008a). A variety of sesquiterpenes have been detected in the atmosphere, including β-caryophyllene, α-humulene, longifolene, α-farnesene, and α-cedrene (Helmig et al., 2007; Sakulyanontvittaya et al., 2008a; Duhl et al., 2008; Bouvier-Brown et al., 2009). Sesquiterpenes have a high SOA forming potential because of their large molecular sizes and, for many of them, the endocyclic double bond structure which favors the formation of low-volatility oxidation products. The results of laboratory chamber studies show high aerosol mass yields (defined as the mass of organic aerosol formed per mass of precursor VOC reacted) from sesquiterpene oxidation (Hoffmann et al., 1997; Lee et al., 2006; Ng et al., 2006; Winterhalter et al., 2009; Chen et al., 2012; Jaoui et al., 2013; Yao et al., 2014; Tasoglou and Pandis, 2015). For example, an average 53% aerosol mass yield was reported for ozonolysis and 55% for photooxidation (Jaoui et al., 2013). Field and model studies have shown that sesquiterpene SOA comprises a significant fraction (6-32%) of ambient organic aerosol from local to regional scales (Sakulyanontvittaya et al., 2008b; Hu et al., 2008; Bouvier-Brown et al., 2009; Ding et al., 2014; Ying et al., 2015), with its contribution comparable to that of monoterpene SOA in a variety of environments including rural, suburban, and urban areas (Hu et al., 2008; Ding et al., 2014).

Although sesquiterpene oxidation contributes substantially to SOA, the underlying mechanisms of SOA formation and growth are not well understood. Previous studies of sesquiterpene oxidation have mainly focused on aerosol mass yields, the identities and formation mechanisms of first-, second-, and higher-generation low molecular weight (LMW) oxidation products, and their contributions to the formation of SOA (Hoffmann et al., 1997; Jaoui et al., 2004, 2013; Lee et al., 2006; Ng et al., 2006; Kanawati et al., 2008; Reinnig et al., 2009; Winterhalter et al., 2009; Li et al., 2011; Chan et al., 2011; Chen et al., 2012; Alfarra et al., 2012; Yao et al., 2014). A few studies have suggested that sesquiterpenes play an important role in new particle formation. For instance, field observations show that in new particle formation events, sesquiterpene oxidation products significantly contribute to initial nucleation and growth (Boy et al., 2008; Bonn et al., 2008). In addition, Bonn and Moortgat (2003) suggested that the formation of oligomers was potentially important for nucleation. Lastly, laboratory studies of the ozonolysis of β-caryophyllene and α-cedrene have reported a negative influence on particle nucleation of species that can scavenge stabilized Criegee intermediate (SCI), supporting a key role for sesquiterpene SCI in forming new particles (Bonn and Moortgat, 2003; Yao et al., 2014).

α-Cedrene (Fig.1) is found in air (Duhl et al., 2008), reacts rapidly with O_3 (Richters et al., 2015), and is also an ideal compound for the study of sesquiterpene oxidation because (1) the single C=C bond in its structure helps to simplify the oxidation chemistry and the product distribution, and (2) its resemblance to other sesquiterpenes such as β-caryophyllene and α-humulene in the endocyclic double bond structure (with a methyl group at one end) may enable, to some degree, the generalization of SOA formation mechanisms for this class of compounds. Previous studies of α-cedrene oxidation identified a number of products with molecular masses below 300 Da in both the gas and particle phases, and proposed reaction mechanisms based on known ozone chemistry (Jaoui et al., 2004, 2013; Reinnig et al., 2009; Yao et al., 2014). Preliminary results from our lab (Zhao et al., 2015) subsequently identified higher molecular weight products in the α-cedrene ozonolysis for the first time, and the SOA composition suggested that the major mechanisms for particle formation are likely different than that for the small alkenes (Sadezky et al., 2008; Zhao et al., 2015).

There have been very few measurements of the phase state of sesquiterpene SOA. The phase state of SOA has an important influence on a number of physical and chemical processes of aerosols, such as formation and growth (Koop et al., 2011; Perraud et al., 2012; Shiraiwa and Seinfeld, 2012; Renbaum-Wolff et al., 2013), chemical aging (Renbaum and Smith, 2009;

Shiraiwa et al., 2011; Lignell et al., 2014; Chan et al., 2014; Slade and Knopf, 2014), and water uptake (Mikhailov et al., 2009; Koop et al., 2011; Bones et al., 2012; Hodas et al., 2015; Pajunoja et al., 2015), and thus affects their environmental and climate impacts. There is ample evidence that in many cases, SOA may not be a low-viscosity liquid but rather a highly viscous semi-solid (Virtanen et al., 2010; Cappa and Wilson, 2011; Koop et al., 2011; Vaden et al., 2011; Saukko et al., 2012; Perraud et al., 2012; Abramson et al., 2013; Renbaum-Wolff et al., 2013; Kidd et al., 2014a, b; Bateman et al., 2015). Recently, Saukko et al. (2012) and Pajunoja et al. (2015) examined the phase state of SOA particles formed from OH and O_3 oxidation of longifolene based on particle bounce measurements and found that longifolene SOA is solid or semi-solid over a wide range of relative humidities. To better understand the phase state of sesquiterpene SOA and its implications for various atmospheric processes, more particle phase state measurements are needed.

In the present study, we report the results of a more comprehensive experimental investigation of ozonolysis of α-cedrene. The phase state and mechanisms of growth of SOA are examined by probing the evaporation of a tracer molecule, 2-ethylhexyl nitrate (2-EHN), incorporated into the SOA during ozonolysis. The structures and formation mechanisms of high molecular weight (HMW) products, as well as their roles in particle formation and growth, are elucidated in light of their fragmentation mass spectra, accurate mass data, size-dependent SOA composition, and the effects of water vapor and SCI scavenger. The identity and formation mechanisms of some newly observed LMW (MW < 300 Da) oxidation products are also explored.

2. Experimental

Experiments on α-cedrene ozonolysis were carried out both in a glass flow reactor and in static Teflon chambers in the absence and presence of water vapor or SCI scavengers at 295 ± 1 K. No seed particles or OH scavengers were used in any of these experiments. Table 1 and Figure S1 summarize the conditions and particle characteristics for various types of flow reactor and chamber experiments.

2.1 Flow reactor experiments

The flow reactor (4.6 cm i.d. and 85 cm long) used in this study has been described in detail previously (Zhao et al., 2015). α-Cedrene was added to the flow reactor by injecting the pure liquid (Sigma-Aldrich and Extrasynthese, > 98%) into a flow of 1.76-2.96 L min^{-1} of clean, dry air (Praxair, ultra zero air) using an automated syringe pump (Pump Systems Inc., model NE-1000). Ozone was generated by passing a flow of O_2 (Praxair, Ultra High Purity, 99.993%) at 0.24 L min^{-1} through a pen-ray mercury lamp (model 11SC-2), and subsequently added to the flow reactor downstream of the α-cedrene inlet. The O_3 concentration, determined using a UV-VIS spectrometer (Ocean Optics, HR4000), was adjusted by changing the UV exposure of the O_2 via a movable metal cover surrounding the lamp. The total flow rate in the reactor was 2.0, 2.9, or 3.2 L min^{-1}, corresponding to a residence time of 44, 30, or 27 s, respectively. Some of the experiments were carried out in the presence of water vapor or formic acid, both of which can act as SCI scavengers. Water vapor was added by bubbling a flow of clean air through nanopure water (18.2 MΩ cm) into the flow reactor. The relative humidity of the airflow (~ 75% RH) in the reactor was measured using a humidity probe (Vaisala, HMT234). Formic acid (Sigma-Aldrich, ≥ 95%) was added to the reactor using the same method as for α-cedrene.

The particle size distributions were measured at the outlet of the reactor using a scanning mobility particle sizer (SMPS, TSI), which is equipped with an electrostatic classifier (model 3080), a long differential mobility analyzer (model 3081) and a condensation particle counter (model 3776). When the size distribution of SOA was stable, the polydisperse particles were collected onto a 47-mm PTFE filter (Millipore Fluoropore, 0.45μm pore size) at a flow rate of 1.9, 2.8, or 3.1 L min^{-1}, with venting of the remaining 0.1 L min^{-1} aerosol flow to the hood. In order to obtain sufficient particle mass for the analysis, the collection lasted 3-15 hours, depending on the particle mass concentrations. Excellent collection efficiency (> 99%) was obtained for particles of all diameters as established by SMPS measurements downstream of the filter. The filter samples were extracted immediately with a 2-mL mixture (5:3 in v/v) of methanol (OmniSolv, LC-MS grade) and hexanes (a mixture of hexane isomers, Fisher Scientific, 99.9%) under ultrasonication in an ice bath for 30 min. The extracts were then purged gently using a flow of dry N_2 at room temperature to evaporate down to 1-mL. As hexanes are more volatile than methanol, the remaining solvent in the extracts would be primarily methanol. The resulting extracts were either analyzed directly using an LCT Premier electrospray ionization time-of-flight mass spectrometer (ESI-ToF-MS, Waters) or diluted with water (OmniSolv, LC-MS grade) to yield a final 50:50 water:methanol mixed solution, followed by analysis with a

Xevo TQS electrospray ionization triple quadrupole mass spectrometer (ESI-TQ-MS, Waters). In order to verify that the sonication has no significant impact on SOA measurements, filter extraction was performed instead, in some experiments, in the mixture of methanol/hexanes by shaking for 30 min. No significant difference in product distribution was observed in ESI mass spectra of the SOA extracted with and without sonication. In separate experiments, the chemical composition of α-cedrene SOA was also measured in real time using direct analysis in real time mass spectrometry (DART-MS).

2.2 Chamber experiments

Chamber experiments were carried out in 450 L Teflon chambers. Two types of α-cedrene ozonolysis experiments were conducted: (i) under dry or humid (72% RH) conditions, and (ii) in the absence or presence of gas phase 2-ethylhexyl nitrate (2-EHN), which was incorporated into SOA during ozonolysis and used as a tracer molecule to probe the viscosity of SOA. The α-cedrene was added using an automated syringe pump to inject a defined volume of pure liquid into a flow of clean, dry air, which was directed into the chamber. Water vapor was added by bubbling air through nanopure water into the chamber. 2-EHN (Sigma-Aldrich, 97%) was added by injecting a known volume of liquid into the chamber. After 10 min to allow for mixing of the gases (or two hours for the evaporation of the 2-EHN), ozonolysis was initiated by adding O_3 generated by a commercial ozone generator (Polymetrics, Model T-816) to the chamber.

For experiments CH1-CH3 (Table 1), SOA composition was examined online by a high resolution time-of-flight aerosol mass spectrometer (HR-ToF-AMS, Aerodyne Research Inc.), or by collection onto a PTFE filter at a flow rate of 12 L min^{-1}. Filter sampling started after 30 min reaction time and lasted about 30 min. Because of the small volume of the chamber (450 L) and relatively low SOA mass loading formed (see Table 1), in each experiment the SOA was sampled onto one filter to ensure enough mass for ESI-MS analysis. The filter was extracted using the same method as for SOA samples obtained in flow reactor experiments, followed by ESI-MS analysis. For experiments CH4 and CH5, SOA formed without or with added 2-EHN at a 60 min reaction time was collected onto a germanium (Ge) attenuated total reflectance (ATR) crystal using a custom designed impactor (Kidd et al., 2014b) at a flow rate of 30 L min^{-1}. The SOA impacted on the ATR crystal was subsequently probed using attenuated total reflectance-Fourier transform infrared (ATR-FTIR) spectroscopy.

Most experiments were performed with excess O_3. In order to evaluate the influence of excess O_3, which could lead to secondary oxidation of first generation products, some experiments were performed with excess α-cedrene (Table 1, experiment CH3). The ESI mass spectra of SOA formed in the presence of excess O_3 or excess α-cedrene are very similar, suggesting that the excess O_3 has no observable influence on SOA formation. In addition, no significant difference was observed in ESI mass spectra of SOA formed with or without added 2-EHN, suggesting that the incorporation of 2-EHN into the SOA does not change its overall composition.

2.3 SOA characterization

In both flow reactor and chamber experiments, aerosol samples were directed through a 10-cm monolith extruded carbon denuder (Novacarb^{TM}; Mast Carbon, Ltd.) to remove the gas phase species prior to particle collection on the filter. No significant difference in particle size distribution was observed with or without the denuder. Blank experiments were also carried out under the same experimental conditions as the ozonolysis experiments but without adding O_3 to the flow reactor or the chamber.

2.3.1 ATR-FTIR measurements

The ATR crystal with impacted SOA was placed immediately into an ATR cell (volume ~ 2 cm^3) located in the sampling compartment of a Nicolet 6700 FTIR spectrometer (Thermo Scientific). A flow of dry synthetic air at 100 mL min^{-1} passed over the sample on the crystal. In some experiments, this flow first passed through a pen-ray mercury lamp, producing 8 ppm O_3, in order to probe the possibility of secondary oxidation of SOA components by O_3. Single beam spectra at a resolution of 4 cm^{-1} (128 scans) were collected before and after impaction of SOA. The absorbance spectra of SOA on the crystal were derived from $\log_{10}(S_0/S_1)$ where S_0 and S_1 represent the single beam spectra of the clean and SOA-covered crystal, respectively. The IR spectra of SOA were obtained over 20 hours of air or O_3 exposure to study the evolution and evaporation of the impacted SOA during this period. In experiments performed in the presence of 2-EHN, the signal at 1280 cm^{-1} was followed over time to investigate the evaporation of 2-EHN and determine its diffusion coefficient throughout the SOA matrix.

2.3.2 ESI-MS measurements

Extracts of both SOA and blank samples were analyzed by ESI-ToF-MS operated in either positive or negative ion mode. The operating conditions of this mass spectrometer were described previously (Zhao et al., 2015). Mass spectra were acquired in the 200-1000 Da mass range. Although ESI often forms multiply charged ions, the major ions observed throughout the mass spectra are in the singly charged state, as indicated by the unity spacing of the isotope peaks (Greaves and Roboz, 2013). Sodium adducts $[M+Na]^+$ were the primary ions observed in the positive ion mode (ESI+) and deprotonated ions $[M\text{-}H]^-$ in the negative ion mode (ESI−). Mass spectra of blanks, in which the peaks are mainly attributed to the impurities in the solvent and filter and have intensities of 10-30% of SOA peaks, were subtracted from those of SOA samples. Accurate mass measurements were performed using sodium formate, polyethylene glycol, and polyethylene glycol monomethyl ether as mass calibration standards. In addition, SOA extracts were analyzed using ESI-TQ-MS to record the fragmentation spectra (MS^2) of selected ions, from which typical structures of reasonable products based on likely mechanisms were tentatively assigned. The parent ions selected by the first quadrupole (Q1) enter the collision cell (Q2), where they fragment via collision-induced dissociation (CID) with argon as the collision gas at collision energies of 20-30 eV, and the resulting fragment ions are monitored by the third quadrupole (Q3). In this case, the ESI source was operated in positive ion mode under optimized conditions as follows: capillary voltage 3.2 kV, desolvation gas flow 1000 L h^{-1}, desolvation gas temperature 500 ^{o}C, nebulizer gas pressure 7 bar.

2.3.3 AMS measurements

An Aerodyne HR-ToF-AMS was used to analyze the chemical composition and to examine O:C ratios of polydisperse SOA formed in the chamber. Due to the small sizes of the SOA formed in the flow reactor, it was impossible to measure them with the AMS, and thus all AMS results presented hereafter are exclusively from the chamber studies. A detailed description of this instrument has been given elsewhere (DeCarlo et al., 2006). The SOA sampled into the instrument was vaporized at 600 ^{o}C. High resolution MS data were collected in both V-mode and W-mode and analyzed using the “Improved-Ambient” method (Canagaratna et al., 2015). Measurements with a particle filter were carried out before each experiment to aid in quantification of the CHO^+ fragment at *m/z* 29 which has interference from gaseous ^{15}NN and can significantly affect elemental analysis.

2.3.4 DART-MS measurements

Direct analysis in real time mass spectrometry (DART-MS) is an atmospheric pressure soft ionization method used to examine chemical composition of solid and liquid samples after thermal desorption. A more detailed description of this mass spectrometric technique is given elsewhere (Cody et al., 2005; Nah et al., 2013). In this work, α-cedrene SOA formed in the flow reactor under dry conditions was measured in real time using a Xevo TQS triple quadrupole mass spectrometer (Waters) equipped with a commercial DART ion source (IonSense, DART SVP with Vapur® Interface). As DART-MS is a surface-sensitive technique, to ensure that the bulk of particles can be effectively probed, the aerosol stream exiting the flow reactor, in which the gas phase species was removed using a denuder, was heated to 160 ^{o}C before entering into the ionization region. The DART ion source was operated in either positive or negative ion modes with He as the reagent gas under the following conditions: He gas flow 3.1 L min^{-1}; He gas temperature 200 ^{o}C; grid electrode voltage 350 V. The configuration of the DART ion source interfaced to the MS is shown in Fig. S2.

3. Results and discussion

3.1 ATR-FTIR measurements

Figure 2a is a typical ATR-FTIR spectrum recorded immediately following impaction of α-cedrene SOA formed in the chamber in the absence of 2-EHN. The strong C=O band at 1706 cm^{-1} suggests that aldehydes/ketones are important SOA components. A shoulder at 1762 cm^{-1} may indicate the presence of carboxylic acids, esters, or other C=O group-containing species with a more electronegative atom such as oxygen being attached to the carbonyl carbon (Socrates, 2001; Kidd et al., 2014a).

Figure 2b is a difference spectrum showing the changes in SOA after exposure to a flow of clean dry air for 20 hours. The positive and negative peaks in the spectrum represent an increase or decrease respectively in the functional groups in SOA due to air exposure. There is a decrease in peaks at 3416, 1762, 1371 and 1076 cm^{-1} and an increase in peaks at 1735, 1706, 1410 and in the 1100-1350 cm^{-1} region. Note that there is no obvious change in the C-H peaks around 2957 cm^{-1}, suggesting that evaporation of organic species from SOA during air exposure is not important. Therefore, the changes in SOA as indicated by the difference spectra are due to chemistry occurring in SOA during air exposure. One of the possible processes is the decomposition of oligomers that comprise a significant fraction of α-cedrene SOA as discussed later. For example, decomposition of peroxyhemiacetals and aldol condensation products to their precursors can lead to the loss of O-H groups and concomitant formation of ketone/aldehyde C=O groups. The decomposition of oligomers in SOA was supported by ESI-MS measurements of SOA collected on Teflon filters and then exposed to a flow of clean dry air; thus the relative ion intensity of oligomers to LMW products in the mass spectrum of SOA extracted after 20 hours of air exposure is ~ 15% lower compared to that of SOA extracted immediately following collection. The difference spectrum of the SOA film exposed to clean humid air at 89% RH for 40 min (Fig. S3) shows a broad band centered at 3426 cm^{-1} and a narrow band at 1640 cm^{-1} resulting from the stretching and bending vibration of adsorbed water respectively, with relative strength of stretching vs. bending of ~ 2. The absence of a negative peak at 1640 cm^{-1} in the difference spectrum after dry air exposure as shown in Fig. 2b, therefore, suggests that the contribution of water to the loss in the O-H band at 3416 cm^{-1} is minor and the decrease in this region must be due to a change in SOA components.

Figure 2c shows the difference spectrum of SOA upon exposure to 8 ppm O_3 for 20 hours which is very similar to the difference spectrum of SOA after 20 hours of clean air exposure (Fig. 2b). This shows that the α-cedrene SOA oxidation products are not reactive toward O_3, at least as detectable by changes in the infrared spectrum.

3.2 Viscosity and phase state of SOA

In order to probe the phase state of α-cedrene SOA, a relatively volatile organic species, 2-ethylhexyl nitrate (2-EHN, $P_{sat} = 1.4 \times 10^{-4}$ atm at 295 K, Pankow and Asher, 2008), was included in one type of experiment (CH-5, Table 1) so that it could be incorporated into the SOA as it is formed in the chamber. The evaporation of 2-EHN from the SOA impacted onto the ATR crystal upon exposure to a flow of clean dry air was followed with time to probe the phase state of SOA.

Figure 3a shows a digital photograph of a typical impaction pattern on the ATR crystal of α-cedrene SOA formed in the chamber in the presence of gas phase 2-EHN. The SOA impacts and adheres to the crystal, forming a narrow film ~ 1.0 mm in width at the centerline. Similar impaction patterns were also observed for the SOA formed without added 2-EHN. Figure 3b shows the SOA number and mass size distributions after 60 min reaction time in the chamber, as well as the collection efficiency of the impactor as a function of particle diameter (Kidd et al., 2014b). By dividing the particles into a number of 10-nm size bins and applying the average particle collection efficiency at each bin, the SOA mass collected on the crystal is estimated to be 42 µg using $\sum m_i f_i$, where m_i and f_i are the particle mass and average particle collection efficiency at each size bin, respectively. Since the particle wall loss in the chamber during impaction was not considered, this mass should be an upper limit. Assuming a particle density of 1.1 g cm^{-3} (Yao et al., 2014), the maximum average thickness of the SOA film on the ATR crystal is estimated to be L = 0.54 µm. This estimate of L relies on the assumption that SOA impacted on the crystal forms a uniform narrow film. This may underestimate the film thickness by as much as a factor of two if, rather than forming a thin film, the SOA is collected in separate columns immediately below the impactor holes. An additional, smaller, uncertainty in L results from variation in the collection efficiency of the impactor over the particle size range of interest (see Fig. 3b). We estimate the combination of these two to give an uncertainty in L of about a factor of two.

The refractive index of α-cedrene SOA is not known but a value of ~ 1.5 is reasonable based on literature values for SOA from other biogenic organic oxidations (Lambe et al., 2013; Kim et al., 2014). The penetration depth of the IR beam at 1280 and 1635 cm^{-1}, peaks which correspond to the absorption bands of organic nitrate as discussed below, is then calculated to be 0.52 and 0.41 µm (Harrick, 1967), respectively, for SOA on a Ge crystal. This suggests that the entire depth of the SOA film on the ATR crystal can be probed reasonably well by the IR beam in the region of interest.

Figure 4a is a typical ATR-FTIR spectrum of α-cedrene SOA formed in the presence of 2-EHN in the chamber under dry conditions. The spectrum is essentially the same as that of SOA formed without 2-EHN (Fig. 2a) except that there are two new bands at 1635 and 1280 cm^{-1} resulting from the vibrations of nitrate (Socrates, 2001; Bruns et al., 2010; Perraud et al., 2012) when 2-EHN is present. Figure 4b shows the difference spectrum of SOA after exposure to a flow of clean dry air for 20 hours. In addition to the spectral features similar to the difference spectrum of 2-EHN-free SOA (Fig. 2b), there is a small loss of nitrate peaks at 1635 cm^{-1} and 1280 cm^{-1}, indicating some evaporation of 2-EHN from SOA during air exposure. Figure 5 shows the temporal evolution of the integrated area of the nitrate peak at 1280 cm^{-1} over 20 hours of air exposure. It can be seen that after 20 hours of air exposure, only ~ 27% of 2-EHN evaporated from the SOA. This slow evaporation indicates that 2-EHN is incorporated in the bulk of the SOA, and that the SOA must be a high-viscosity semi-solid rather than a liquid where diffusion would be much more rapid (Shiraiwa et al., 2011; Koop et al., 2011).

The incorporation of high-volatility 2-EHN into the bulk of high-viscosity SOA is consistent with a condensation particle growth mechanism (Finlayson-Pitts and Pitts, 2000; Seinfeld and Pandis, 2006; Riipinen et al., 2011; Perraud et al., 2012), for which organic species condense kinetically onto the surface of pre-existing particles and become buried and incorporated into the bulk by incoming low volatility organics. It is important to note that in the ATR-FTIR spectrum (Fig. 4c) of α-cedrene SOA formed without added 2-EHN in the chamber and then exposed to 20 ppm 2-EHN in the ATR cell for one hour, the absorption bands associated with organic nitrate at 1635 and 1280 cm^{-1} are negligible. This observation suggests that the uptake of 2-EHN into or onto previously formed SOA is not important.

Assuming that the evaporation of 2-EHN is determined only by its diffusion in the film of SOA impacted on the ATR crystal and that the diffusion follows Fick's Law, for a film with uniform 2-EHN concentration (C_0) at t = 0 and zero concentration at the surface for t > 0, the total fraction (F) of 2-EHN remaining in the film at time t can be expressed as (Crank, 1975; Mehrer, 2007)

$$F = \frac{8}{\pi^2}\sum_{j=0}^{\infty}\frac{1}{(2j+1)^2}\exp\left[-\frac{(2j+1)^2\pi^2 Dt}{4L^2}\right] \qquad j = 0, 1, 2, \cdots \tag{1}$$

In eq. (1), *D* is the diffusion coefficient of 2-EHN in the SOA and *L* is the thickness of the SOA film on the ATR crystal. A best fit of the evaporation data of 2-EHN in Fig. 5 to eq. (1) gives $D/L^2 = 5.6 \times 10^{-5}$ min^{-1}. With the SOA film thickness *L* of 0.54 μm estimated above, the diffusion coefficient (*D*) of 2-EHN in SOA is calculated to be 3×10^{-15} cm^2 s^{-1}, consistent with the *D* values of the order of ~ 10^{-15} cm^2 s^{-1} predicted from the time scale for evaporation combined with the estimated thickness of the SOA layer (Shiraiwa et al., 2011; Koop et al., 2011). The uncertainty in *L* of about a factor of two described above translates into an uncertainty in *D* of about a factor of four. However, this value for *D* is within the range of diffusion coefficients that would be expected in a highly viscous semi-solid matrix, i.e., $D = 10^{-10}$ $–10^{-20}$ cm^2 s^{-1} (Shiraiwa et al., 2011; Koop et al., 2011), confirming that α-cedrene SOA is a high-viscosity semi-solid. However, because of their small sizes, these particles do not have enough momentum to bounce as they impact on the ATR crystal, as seen for larger SOA from α-pinene oxidation in earlier studies (Kidd et al., 2014a, b). Recently, Saukko et al. (2012) and Pajunoja et al. (2015) reported the formation of semi-solid SOA from the oxidation of the sesquiterpene longifolene based on particle bounce measurements. However, to our knowledge, the present work shows the first measurement of the diffusion coefficient of an organic species in sesquiterpene SOA.

3.3 SOA composition

Figure 6 shows typical ESI+ and ESI− mass spectra of SOA formed from α-cedrene ozonolysis in the flow reactor at 30 s reaction time. Ions in the mass range *m/z* 220-350 correspond to low molecular weight (LMW) products derived directly from oxidation of α-cedrene and retaining much of the structure of the parent compound (hereafter termed P1 products). Those with *m/z* > 420 correspond to high molecular weight (HMW) products formed using two, three, or four P1 products (hereafter termed P2, P3, and P4 products, respectively) as building blocks. We try to avoid using the terms "dimer", "trimer", etc. which may imply simple combinations of smaller species whereas P2, P3, etc. are clearly complex combinations of different LMW products. As discussed above, there is no evidence that any of these peaks arise from multiple charging of higher molecular weight species. The data presented in Fig. 6 suggest that P1 and P2 products comprise a dominant fraction of α-cedrene SOA. Compared to the ESI+ spectrum, the corresponding ions in the ESI− spectrum are generally 24 Da lower in mass. This is consistent with the fact that the ions observed in the ESI+ mode are primarily sodium adducts while those in the ESI− mode are deprotonated ions with a predominant contribution from carboxylic acids.

Figure 7 shows the ESI mass spectra of polydisperse α-cedrene SOA (size distributions are given in Fig. S1a) with geometric mean diameters of 15 and 23 nm formed in the flow reactor at the same concentrations of α-cedrene and O_3 but different reaction times (27 s and 44 s) under dry conditions (Table 1, experiments FR1-FR2). Among P2 products, those at m/z 481-543 are the most abundant ones in the flow reactor SOA and they have a greater contribution to the smaller particles formed at shorter reaction times (Fig. 7a). Conversely, P1 products contribute more to larger particles formed at longer reaction times (Fig. 7b). Figure S4 shows additional ESI mass spectra of polydisperse α-cedrene SOA particles of different geometric mean diameters (13, 18, and 26 nm) formed in the flow reactor at the same reaction time (30 s) but different concentrations of α-cedrene under dry conditions (Table 1, experiments FR3-FR5). A similar size-dependent distribution of P1 and P2 products is observed. These results suggest that P2 products at *m/z* 481-543 may play an important role in initial particle formation, while P1 products contribute significantly to particle growth.

Figure 8 shows typical ESI+ and ESI− mass spectra of α-cedrene SOA formed in the chamber. The chamber SOA has a geometric mean diameter of 66 nm, larger than those formed in the flow reactor (13-26 nm, depending on the experimental conditions) due to the longer reaction times and hence greater extents of reaction. Figure 8 shows that the chamber particles also have relatively more P1 products, in agreement with the important role of P1 products in particle growth. In addition, the subset of P2 products with m/z > 543 in the positive ion mode account for a greater fraction of total P2 products in the chamber SOA than in the flow reactor SOA (Figs. 6a and 7). This suggests that these larger P2 products (i.e., m/z > 543) are mainly formed at longer reaction times in the chamber and contribute mainly to particle growth.

It is known that P1 products may undergo ion-molecule reactions to form noncovalently bound clusters in the ESI source (Muller et al., 2009; Gao et al., 2010), and the formation of such clusters, if it occurs, is expected to be positively correlated with the abundance of P1 products. However, as shown in Figs. 7 and S4, the signal intensity ratio of P2 to P1 products is inversely dependent on the size of SOA. This suggests that the P2 products observed in ESI mass spectra are unlikely to be artifacts of in-source clustering. In addition, HMW products in α-cedrene SOA are also detected in real time by DART-MS that employs a different ionization method. Figure S5 shows typical DART+ (positive ion mode) and DART− (negative ion mode) mass spectra of flow reactor α-cedrene SOA, which was heated to 160 ^{o}C before introduction into the ionization region. The masses of P1 and P2 products in the DART+ mass spectrum are generally 22-24 Da lower than those in the ESI+ mass spectrum (Fig. 6), consistent with the ions detected by DART-MS in the positive mode being primarily $[M+H]^+$, M^+, and $[M-H]^+$ (Cody et al., 2005; Nah et al., 2013). In contrast, essentially the same masses for P1 and P2 products were observed in DART− and ESI− mass spectra, in both of which the ions are predominantly $[M-H]^-$. There are some differences between ESI and DART mass spectra that are likely due to the heating of incoming aerosol stream for DART-MS and the higher DART source temperature. Overall, DART-MS measurements further support that the P2 products observed by ESI-MS are not artifacts from the ion source.

Previous studies have reported an OH yield of 62-67% from ozonolysis of α-cedrene (Shu and Atkinson, 1994; Yao et al., 2014). Therefore, reaction with OH could play a role in α-cedrene oxidation in the absence of an OH scavenger. We reported in a previous study (Zhao et al., 2015) ESI-MS spectra in the absence and presence of cyclohexane, which showed that the relative intensity of P2-P4 peaks in the presence of cyclohexane is smaller. This suggests that OH oxidation may contribute to the formation of HMW species.

Possible structures and formation mechanisms of typical P1 and P2 products (as labeled in Fig. 6) were explored based on their fragmentation mass spectra (MS^2), accurate mass data, previously identified P1 products (Jaoui et al., 2004, 2013; Reinnig et al., 2009; Yao et al., 2014), and likely reaction mechanisms of terpene ozonolysis. To the best of our knowledge, this is the first detailed examination of HMW products initially reported (Zhao et al., 2015) in this system.

3.3.1 P1 products.

The characterization of the molecular structures and formation mechanisms of P1 products from the ozonolysis of α-cedrene has been the emphasis of earlier studies (Jaoui et al., 2004, 2013; Reinnig et al., 2009; Yao et al., 2014). A number of multifunctional P1 products were tentatively identified using different mass spectrometric and derivatization techniques in those studies. Figure S6 shows the ESI(+)-MS^2 spectra as well as the proposed structures of the products with *m/z* values in the range of 245-291 Da measured in the current experiments. As reported by Tolocka et al. (2004), fragmentation of sodium adducts is difficult so the product ion intensities are relatively weak. However, fragmentation is seen to occur mainly via loss of 18 Da (H_2O, indicating the presence of an aldehyde, carboxylic or hydroxyl group), loss of 30 Da (CH_2O, indicating the presence of a formyl group), loss of 32 Da (CH_4O, indicating the presence of a hydroxymethyl group), loss of 44 Da (CO_2 or C_2H_4O, indicating a carboxylic or acetyl group), and loss of 46 Da (CH_2O_2, indicating a carboxylic group). The fragmentation pathways of the functional groups as shown here generally agree with those reported in the literature (Tolocka et al., 2004; Hall and Johnston, 2012), where ESI-MS in positive ion mode was used to characterize the structure of reaction products from ozonolysis of α-pinene. The structures assigned to the products at *m/z* 245-291 are consistent with those reported in the previous studies (Jaoui et al., 2004, 2013; Reinnig et al., 2009; Yao et al., 2014). In many cases, the MS^2 spectra can be due to multiple isomeric structures. Table 2 shows accurate mass data for these P1 products. Their measured accurate masses are for the most part in excellent agreement with the elemental formulae for their proposed structures, the exception being P1-289 in the negative ion mode.

In addition to the products reported previously (Jaoui et al., 2004, 2013; Reinnig et al., 2009; Yao et al., 2014), some products corresponding to the $[M+Na]^+$ at *m/z* 305-323 not previously identified were detected by ESI-MS. Figure S7 shows the parent ion spectra of these sodiated ions at collision gas energy (CE) of 6 eV that is equivalent to the CE for MS scan. Parent ion spectra of *m/z* 305-323 have negligible parents but strong signals from themselves at this low CE. This strongly suggests that these ions are molecular ions rather than fragments from larger products. However, as shown in the insets of Fig. S7, significant parents are observed for these ions when the CE is increased to 20 eV. This is reasonable since these P1 products can be precursors of HMW products, which is expected to fragment readily back to its precursors at higher CEs, and that the fragmentation of HMW products formed from other P1 products is also likely to give fragments with *m/z* values of 305-323. These P1 products were also observed by DART-MS in the *m/z* 281-301 region primarily as $[M+H]^+$ with some contribution from $[M]^+$ in the positive ion mode, or $[M-H]^-$ ions in the negative ion mode (Fig. S5), consistent with DART-MS studies of single compounds (Nah et al., 2013).

Figure 9 shows the potential structures of these newly observed P1 products proposed based on their ESI-MS^2 spectra (Fig. S8). The fragments resulting from the loss of water and multiple oxygenated functional groups such as carboxylic, carbonyl, and hydroxyl groups were observed. It was found in our previous study that the formation of the products corresponding to *m/z* 305-323 ions continues in the presence of cyclohexane as an OH scavenger (Zhao et al., 2015). This suggests that the newly observed products are not formed by OH oxidation, but rather by O_3 oxidation. Figure S9 illustrates some potential formation mechanisms for these newly observed products. The Criegee intermediates (CIs) form peroxy (RO_2) radicals via the vinyl hydroperoxide (VHP) channel. The conversion of RO_2 to alkoxy (RO) radicals and the subsequent intramolecular H-abstraction/O_2 addition lead again to RO_2 radicals, which can further undergo similar reactions to form RO_2 radicals with higher oxygen content. Termination reactions with RO_2 or HO_2 radicals lead to the formation of the newly observed products.

While accurate mass data of these products (Table 2) agree well with the proposed structures, there may be additional structures and reaction pathways in the formation of the P1 products at *m/z* 305-323 via the VHP channel of CIs that contribute to these peaks. For example, because of their large carbon skeleton, RO radicals may have multiple isomerization pathways to form different structures with the same elemental composition.

Secondary ozonides formed through intramolecular reactions of SCI were observed as the major gas phase products from ozonolysis of α-cedrene (Yao et al., 2014) and β-caryophyllene (Winterhalter et al., 2009), with their formation being significantly suppressed by the addition of water vapor. In the present study, although a sodiated ion with m/z 275 and elemental composition of $C_{15}H_{24}O_3Na$, consistent with the mass and formula of the intramolecularly formed SOZ, was observed in ESI (+) mass spectra of α-cedrene SOA, as will be discussed in Sect. 3.4, the relative intensity of this ion in the mass spectra does not decrease at all at 75% RH and is still pronounced with high concentrations of formic acid (15 ppm) added as an SCI scavenger. This indicates that the ion at m/z 275 is unlikely to be the SOZ. Similarly, Yao et al. (2014) did not observe the SOZ in the particle phase using HPLC-MS and GC-MS. A possible explanation is that the intramolecularly formed SOZ has a relatively high vapor pressure (1.2×10^{-6} atm at 295 K) and therefore a low potential to partition to the particle phase.

3.3.2 P2 products.

Table 2 gives the accurate masses and elemental formulae of the most abundant P2 products as labeled in the ESI mass spectra (Fig. 6a). Figure 10 shows the proposed potential structures of these products based on their accurate mass data and ESI-MS^2 spectra (Fig. S10) (see Supplement for the detailed discussion). These structures include aldol condensation products (formed from the reaction of two carbonyl compounds, Reaction R1), peroxyhemiacetals (formed from the reaction of a carbonyl compound and an organic hydroperoxide, Reaction R2), and esters (formed from the reaction of a carboxylic acid with an alcohol, Reaction R3), with the building blocks being the P1 products typically observed in the SOA.

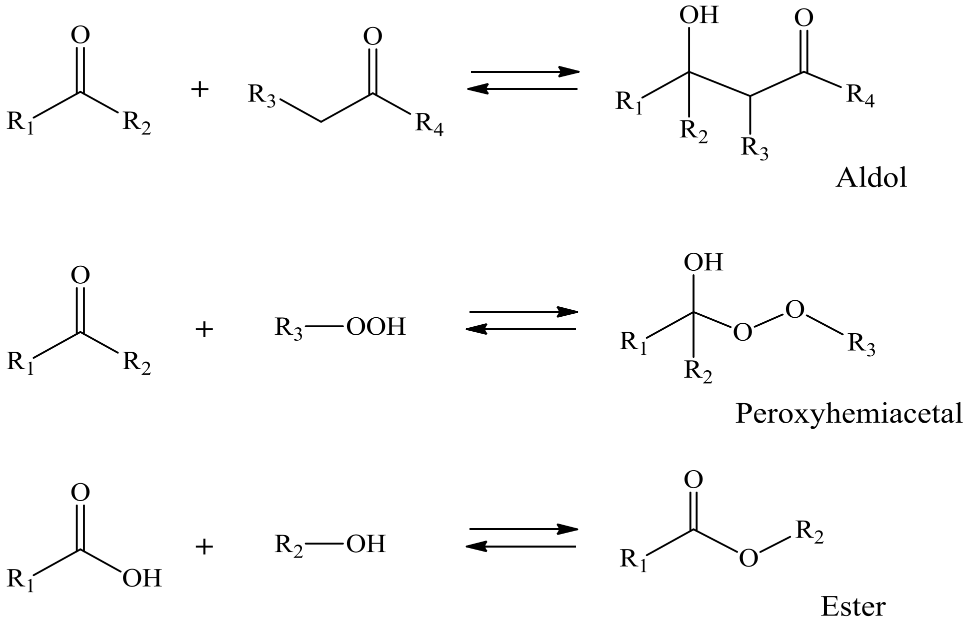

(R1)

(R2)

(R3)

Aldol condensation products and peroxyhemiacetals are the most commonly identified structures. Of 17 proposed structures for these P2 products, ten are aldol condensation products and five are peroxyhemiacetals. Except for products P2-481 and P2-497 that are identified as aldol condensation products, other P2 products may have contributions from multiple structures. For example, product P2-511 may have contributions from both aldol condensation products and esters, and products P2-513, P2-527, and P2-543 may have contributions from both aldol condensation products and peroxyhemiacetals. Although no detailed data concerning the formation of such HMW products during sesquiterpene ozonolysis are available in the literature, a number of laboratory and field studies have found that aldol condensation products, peroxyhemiacetals, and esters are the major HMW products detected in the SOA formed from ozonolysis of monoterpenes (e.g., α-pinene and β-pinene) (Hoffmann et al., 1998; Tolocka et al., 2004; Docherty et al., 2005; Muller et al., 2008, 2009; Heaton et al., 2009; Gao et al., 2010; Yasmeen et al., 2010; Hall and Johnston, 2012; Kristensen et al., 2013, 2014; Witkowski and Gierczak, 2014; X. Zhang et al., 2015). Formation of such products has traditionally been thought to occur via acid-catalyzed reactions (reactions R1-R3) in the condensed phase (Kroll and Seinfeld, 2008; Hallquist et al., 2009; Yasmeen et al., 2010; Ziemann and Atkinson, 2012), although some recent studies suggested that such a process is not favored for esterification in SOA (Birdsall et al., 2013; DePalma et al., 2013; Kristensen et al., 2014; X. Zhang et al., 2015). Formation of peroxyhemiacetals has also been suggested to be thermodynamically favorable in the gas phase (DePalma et al., 2013), although whether the kinetics are sufficiently fast is not known. It is noted that there may be some decomposition of HMW products over time, for example, over 20 hours of clean air exposure as discussed earlier.

3.4 The effects of water vapor and SCI scavenger

The reaction of α-cedrene with ozone has a very high SCI yield (> 88%) (Yao et al., 2014). If SCI reactions are key to SOA formation in this system, the addition of SCI scavengers such as water vapor and formic acid should have significant influence on the formation of SOA.

Figure 11 shows the size distributions of SOA formed from ozonolysis of α-cedrene in the flow reactor under dry conditions, at 75% RH, or in the presence of 15 ppm formic acid. SOA with very similar number concentrations is formed with or without added water vapor, while significantly fewer, but larger, particles are formed in the presence of formic acid. Recent kinetics measurements of the CH_2OO CI reaction with water vapor (monomer and dimer) give rate constants of $k_{dimer} = (4.0 - 6.5) \times 10^{-12}$ cm^3 molecule^{-1} s^{-1} (Chao et al., 2015; Lewis et al., 2015) and $k_{monomer} = 3.2 \times 10^{-16}$ cm^3 molecule^{-1} s^{-1} (Berndt et al., 2015). The rate constant for the reaction of CH_2OO with formic acid is much larger, $k_{HCOOH} = 1 \times 10^{-10}$ cm^3 molecule^{-1} s^{-1} (Welz et al., 2014). The reactivity of Criegee intermediates has been shown to depend on structure for a number of reasons, including different extents of pressure stabilization of excited CI, different reactivities for the *syn*- and *anti*- forms, and different natures of the groups attached to the central CI carbon (Ryzhkov and Ariya, 2004; Anglada et al., 2011; Donahue et al., 2011; Vereecken et al., 2012; Taatjes et al., 2013; Welz et al., 2014). While the α-cedrene CI is clearly very different than CH_2OO, if the rate constants for the latter are representative in a relative sense, the ratio of the rates for reaction of the α-cedrene CI with formic acid and water dimer relative to water monomer are ~ 240: 18: 1 under our experimental conditions (3.7×10^{14} HCOOH cm^{-3}, 4.8×10^{17} H_2O cm^{-3} and 5.1×10^{14} $(H_2O)_2$ cm^{-3}, based on a water equilibrium constant of 0.0536 atm^{-1} (Ruscic, 2013)). Thus, it is not surprising that formic acid has a much greater impact than water. Furthermore, the large effects of formic acid further support the importance of the α-cedrene CI in SOA formation. These impacts of water and formic acid are in agreement with those reported by Yao et al. (2014) who reported a similar quenching effect of added acetic acid on particle formation in the α-cedrene ozonolysis, but relatively little impact of water vapor.

Figures 12a and 12b show the ESI mass spectra of α-cedrene SOA formed in the flow reactor without and with added water vapor, respectively. There are no significant differences in product distribution with and without added water vapor. In addition, ESI-MS^2 measurements show that typical P1 and P2 products as labeled in both mass spectra have very similar MS^2 spectra, suggesting that the product composition is not impacted by the presence of water. Measurements of the chamber SOA by AMS (see Fig. S11) also did not show significant differences in the particle mass spectra upon water addition. On the other hand, Figure 12c shows the ESI mass spectra of SOA formed in the presence of 15 ppm formic acid. The formation of HMW products is significantly reduced as are the number of peaks in the P1 product region. However, P1 products at *m/z* 259, 275, and 291, as well as P2 products, for example, at m/z 527, 543, and 559, are still evident. All of these P1 products have very similar MS^2 spectra (and thus likely similar structures) to those formed in the absence of formic acid. In contrast, P2 products at *m/z* 527 and 543 show significantly different MS^2 spectra compared to those obtained without added formic acid.

Yao et al. (2014) reported an increase in the formation of α-cedronaldehyde in the presence of acetic acid, consistent with an increase in the present studies in the relative abundance of the P1 product at *m/z* 259 assigned to α-cedronaldehyde when formic acid was added (Fig. 12c). The reaction of α-cedrene SCI with formic acid is expected to form α-formyloxy hydroperoxide (MW 298 Da), which is believed to contribute to SOA growth. While the corresponding sodium adduct at *m/z* 321 is not observed in the mass spectrum, this is not surprising as hydroperoxides are likely to undergo decomposition during SOA sampling and analysis (Witkowski and Gierczak, 2013).

Comparison of Fig. 12c to Fig.12a shows that HMW products (P2-P4) formed with added formic acid are less important than those produced in the absence of formic acid. Combined with the smaller number concentration (Fig. 11), the data suggest that HMW products must be important in new particle formation. As fewer particles are formed with the addition of formic acid, more P1 products are available for each particle to grow to larger sizes.

3.5 Mechanisms

The size-dependent composition of α-cedrene SOA and the effect of SCI scavengers on particle formation suggest that HMW products (P2-P4) play an important role in the initial stages of particle formation. This is consistent with earlier suggestions in simpler systems that higher molecular weight products of alkene ozonolysis are primarily responsible for nucleation, while many different products from low to high molecular weight can contribute to growth (Lee and Kamens, 2005; Sadezky et al., 2008; Winkler et al., 2012; Zhao et al., 2013; Ehn et al., 2014; Kidd et al., 2014a; Zhao et al., 2015; X. Zhang et al., 2015). Bonn and Moortgat (2003) estimated an upper limit for the saturated vapor pressure (P_{sat}) of nucleating species produced from sesquiterpene ozonolysis to be 1.2×10^{-13} atm. Donahue et al. (2013) also suggested that organic vapors with $P_{\mathrm{sat}} < 10^{-13}$ atm may contribute to particle nucleation. The P_{sat} of typical P1 products, as well as the P2 products (e.g., ester and peroxyhemiacetal) are estimated by averaging the predictions (see Table S1) from two group contribution methods, SIMPOL.1 (Pankow and Asher, 2008) and EVAPORATION (Compernolle et al., 2011), and are shown in Figure 13. The P_{sat} for the P2 products are 3-6 orders of magnitude lower than the suggested nucleation threshold, consistent with their important contributions to initial particle formation. The newly observed products (P1-321 and P1-323) also have vapor pressures lower than the nucleation threshold and thus may in principle also contribute to nucleation. This is also expected to be the case for the HMW P3 and P4 products. However, without information on their chemical composition and structures, data on P3 and P4 could not be included in Fig. 13. In contrast, the smaller, more volatile P1 products will mainly contribute to particle growth, as suggested by their relatively larger abundance in ESI mass spectra of larger particles (Figs. 7 and S4).

Compared to P2 products at *m/z* 481-543, those with *m/z* > 543 are significantly less important in the flow reactor SOA (geometric mean diameter 13-26 nm), but contribute a greater fraction to total P2 products in the chamber SOA (geometric mean diameter 66 nm). This suggests that these larger P2 products (i.e., *m/z* > 543) play an important role in particle growth and may be formed mainly via condensed phase reactions of P1 products in the SOA.

Elemental analysis of SOA from chamber experiments using AMS results in an average O/C ratio of 0.34 ± 0.03 (1σ) and H/C ratio of 1.51 ± 0.02. These values are within the range given for P1 products detected by ESI-MS (Table 2) and are consistent with our observation that P1 products predominantly contribute to particle growth. Along with the potential mechanisms discussed above to explain the formation of observed P1 and P2 products and their contribution to particle formation and growth, another mechanism considered for particle formation and growth is the production of extremely low-volatility organic compounds (ELVOCs), which was proposed to occur via sequential intramolecular hydrogen abstraction/O_2 addition of RO_2 radicals (Vereecken et al., 2007; Crounse et al., 2013; Ehn et al., 2014; Rissanen et al., 2015) and shown to play an important role in particle formation and growth from monoterpene oxidation (Zhao et al., 2013; Ehn et al., 2014; Jokinen et al., 2015). Because of the high oxygen content in ELVOCs, particles formed from these compounds are expected to have high O/C ratios. The ELVOC mechanism cannot be ruled out as being involved in initial particle formation during α-cedrene ozonolysis. However, based on the O/C ratios measured for chamber SOA, it is unlikely to be a dominant contributor to total particle mass in this system. Measurements by AMS are not possible for the flow reactor experiments as the particles are too small to be efficiently transmitted into the AMS.

It is clear from the impact of formic acid on particle formation that the SCI plays a key role in forming the HMW products and new particles. In the case of the *trans*-3-hexene ozonolysis (Sadezky et al., 2008; Zhao et al., 2015), the composition of the SOA clearly showed evidence for oligomer formation from the sequential reaction of RO_2 radicals with SCI, leading to ESI mass spectra that showed the repeat unit of oligomers corresponding to SCI. A search for similar products in the α-cedrene reaction was not successful, indicating that while this may contribute, other mechanisms are more important (Zhao et al., 2015). This is not surprising, given the number of potential reaction paths for the SCI from α-cedrene (e.g. Fig. S9) and the large number of low volatility products that can quickly contribute to growth and the SOA composition once nucleation has occurred.

The incorporation of 2-EHN into SOA and its very slow evaporation back out (Figs. 4 and 5) is consistent with a condensation type of growth mechanism (Finlayson-Pitts and Pitts, 2000; Seinfeld and Pandis, 2006) in which organic species are irreversibly taken up by the particle surface and thus their incorporation into particles depends on the collision frequency of the gas with the particle surface and the magnitude of the uptake coefficient (Perraud et al., 2012). Such a growth mechanism is characteristic of highly viscous SOA, in which incorporated organic species undergo very slow evaporation because of the diffusion limitation, in contrast to an equilibrium mechanism that applies for low-viscosity liquid particles. This result also suggests that growth will occur not only via low volatility products but also via uptake of higher volatility species such as the smaller P1 products identified here.

4. Summary

The present study examines the phase state and mechanisms of formation and growth of SOA from ozonolysis of α-cedrene. The SOA is characterized to be a high-viscosity semi-solid, with an estimated diffusion coefficient of 3×10^{-15} cm^2 s^{-1} for 2-EHN that was incorporated into the SOA during ozonolysis. High molecular weight products, tentatively identified mainly as aldol condensation products, peroxyhemiacetals, and esters, comprise a significant fraction of SOA. The size-dependent distribution of these products in the SOA as well as their positive correlation with new particle formation suggests that they are responsible for initial particle formation, in contrast to lower molecular weight (P1) products that mainly contribute to particle growth via a kinetic condensation mechanism.

Bonn and Moortgat (2003) have suggested that sesquiterpene ozonolysis could be one source of new particle formation in the boreal forest. Evidence for the role of sesquiterpenes in atmospheric new particle formation has been recently presented by field observations in the boreal forest in Finland (Bonn et al., 2008) and in the Front Range of the Colorado Rocky Mountains (Boy et al., 2008). These studies have proposed possible nucleation mechanisms involving low-volatility products such as intermolecularly formed SOZ and organosulfates from sesquiterpene oxidation. The results of the present study suggest that the formation of HMW products during ozonolysis may serve as an important mechanism for such new particle formation.

Mechanisms of ozonolysis of alkenes and in particular, the pathways that lead to SOA formation are highly dependent on the size and structure of the parent alkene. However, in all cases stabilized Criegee intermediates play a key role. For example, SOA generated from ozonolysis of small alkenes such as *trans*-3-hexene is primarily composed of oligomers formed from the sequential addition of SCI to RO_2 radicals (Sadezky et al., 2008; Zhao et al., 2015). For larger alkenes, such as α-cedrene, the SCI react via multiple pathways, leading to a variety of low volatility products (e.g., P2 and newly observed P1 products) that can nucleate on their own to form new particles. There is yet a third group of alkenes with intermediate molecular sizes such as monoterpenes, for which the major first generation ozonolysis products do not have low enough volatilities to nucleate on their own (Hallquist et al., 2009) and therefore the ELVOC mechanism, despite the small yields (a few percent, Jokinen et al., 2015), may play a more dominant role (Zhao et al., 2013; Ehn et al., 2014). The dependence of phase, composition, and mechanisms for particle formation and growth should be taken into account in atmospheric models of the formation and impacts of SOA on visibility, human health, and climate.

Acknowledgements

This work was supported by the National Science Foundation (Grants #1207112) and the NSF Major Research Instrumentation (MRI) program (Grant # 0923323 and 1337080). The authors are grateful to John Greaves, Beniam Berhane, and Shirin Sorooshian for their help with accurate mass measurements.

References

Abramson, E., Imre, D., Beranek, J., Wilson, J., and Zelenyuk, A.: Experimental determination of chemical diffusion within secondary organic aerosol particles, Phys. Chem. Chem. Phys., 15, 2983-2991, doi:10.1039/C2cp44013j, 2013.

Alfarra, M. R., Hamilton, J. F., Wyche, K. P., Good, N., Ward, M. W., Carr, T., Barley, M. H., Monks, P. S., Jenkin, M. E., Lewis, A. C., and McFiggans, G. B.: The effect of photochemical ageing and initial precursor concentration on the composition and hygroscopic properties of beta-caryophyllene secondary organic aerosol, Atmos. Chem. Phys., 12, 6417-6436, doi:10.5194/acp-12-6417-2012, 2012.

Anglada, J. M., Gonzalez, J., and Torrent-Sucarrat, M.: Effects of the substituents on the reactivity of carbonyl oxides. A theoretical study on the reaction of substituted carbonyl oxides with water, Phys. Chem. Chem. Phys., 13, 13034-13045, doi:10.1039/c1cp20872a, 2011.

Bateman, A. P., Bertram, A. K., and Martin, S. T.: Hygroscopic Influence on the Semisolid-to-Liquid Transition of Secondary Organic Materials, J. Phys. Chem. A, 119, 4386-4395, doi:10.1021/jp508521c, 2015.

Berndt, T., Kaethner, R., Voigtlander, J., Stratmann, F., Pfeifle, M., Reichle, P., Sipila, M., Kulmala, M., and Olzmann, M.: Kinetics of the unimolecular reaction of CH_2OO and the bimolecular reactions with the water monomer, acetaldehyde and acetone under atmospheric conditions, Phys. Chem. Chem. Phys., 17, 19862-19873, doi: 10.1039/c5cp02224j, 2015.

Birdsall, A. W., Zentner, C. A., and Elrod, M. J.: Study of the kinetics and equilibria of the oligomerization reactions of 2-methylglyceric acid, Atmos. Chem. Phys., 13, 3097-3109, doi:10.5194/acp-13-3097-2013, 2013.

Bones, D. L., Reid, J. P., Lienhard, D. M., and Krieger, U. K.: Comparing the mechanism of water condensation and evaporation in glassy aerosol, Proc. Natl. Acad. Sci. U. S. A., 109, 11613-11618, 2012.

Bonn, B., and Moortgat, G. K.: Sesquiterpene ozonolysis: Origin of atmospheric new particle formation from biogenic hydrocarbons, Geophys. Res. Lett., 30, 1585, doi:10.1029/2003GL017000, 2003.

Bonn, B., Kulmala, M., Riipinen, I., Sihto, S. L., and Ruuskanen, T. M.: How biogenic terpenes govern the correlation between sulfuric acid concentrations and new particle formation, J. Geophys. Res., 113, D12209, doi:10.1029/2007jd009327, 2008.

Bouvier-Brown, N. C., Goldstein, A. H., Gilman, J. B., Kuster, W. C., and de Gouw, J. A.: In-situ ambient quantification of monoterpenes, sesquiterpenes, and related oxygenated compounds during BEARPEX 2007: implications for gas- and particle-phase chemistry, Atmos. Chem. Phys., 9, 5505-5518, 2009.

Boy, M., Karl, T., Turnipseed, A., Mauldin, R. L., Kosciuch, E., Greenberg, J., Rathbone, J., Smith, J., Held, A., Barsanti, K., Wehner, B., Bauer, S., Wiedensohler, A., Bonn, B., Kulmala, M., and Guenther, A.: New particle formation in the front range of the colorado rocky mountains, Atmos. Chem. Phys., 8, 1577-1590, 2008.

Bruns, E. A., Perraud, V., Zelenyuk, A., Ezell, M. J., Johnson, S. N., Yu, Y., Imre, D., Finlayson-Pitts, B. J., and Alexander, M. L.: Comparison of FTIR and particle mass spectrometry for the measurement of particulate organic nitrates, Environ. Sci. Technol., 44, 1056-1061, doi:10.1021/Es9029864, 2010.

Canagaratna, M. R., Jimenez, J. L., Kroll, J. H., Chen, Q., Kessler, S. H., Massoli, P., Ruiz, L. H., Fortner, E., Williams, L. R., Wilson, K. R., Surratt, J. D., Donahue, N. M., Jayne, J. T., and Worsnop, D. R.: Elemental ratio measurements of organic compounds using aerosol mass spectrometry: characterization, improved calibration, and implications, Atmos. Chem. Phys., 15, 253-272, doi:10.5194/acp-15-253-2015, 2015.

Cappa, C. D., and Wilson, K. R.: Evolution of organic aerosol mass spectra upon heating: implications for OA phase and partitioning behavior, Atmos. Chem. Phys., 11, 1895-1911, doi:10.5194/acp-11-1895-2011, 2011.

Chan, M. N., Surratt, J. D., Chan, A. W. H., Schilling, K., Offenberg, J. H., Lewandowski, M., Edney, E. O., Kleindienst, T. E., Jaoui, M., Edgerton, E. S., Tanner, R. L., Shaw, S. L., Zheng, M., Knipping, E. M., and Seinfeld, J. H.: Influence of aerosol acidity on the chemical composition of secondary organic aerosol from beta-caryophyllene, Atmos. Chem. Phys., 11, 1735-1751, doi:10.5194/acp-11-1735-2011, 2011.

Chan, M. N., Zhang, H. F., Goldstein, A. H., and Wilson, K. R.: Role of water and phase in the heterogeneous oxidation of solid and aqueous succinic acid aerosol by hydroxyl radicals, J. Phys. Chem. C, 118, 28978-28992, doi:10.1021/jp5012022, 2014.

Chao, W., Hsieh, J. T., Chang, C. H., and Lin, J. J. M.: Direct kinetic measurement of the reaction of the simplest Criegee intermediate with water vapor, Science, 347, 751-754, doi:10.1126/science.1261549, 2015.

Chen, Q., Li, Y. L., McKinney, K. A., Kuwata, M., and Martin, S. T.: Particle mass yield from beta-caryophyllene ozonolysis, Atmos. Chem. Phys., 12, 3165-3179, doi:10.5194/acp-12-3165-2012, 2012.

Cody, R. B., Laramee, J. A., and Durst, H. D.: Versatile new ion source for the analysis of materials in open air under ambient conditions, Anal. Chem., 77, 2297-2302, doi:10.1021/ac050162j, 2005.

Compernolle, S., Ceulemans, K., and Muller, J. F.: EVAPORATION: A new vapour pressure estimation method for organic molecules including non-additivity and intramolecular interactions, Atmos. Chem. Phys., 11, 9431-9450, 2011.

Crank, J.: The mathematics of diffusion, 2nd ed., Clarendon Press, Oxford, [Eng], 1975.

Crounse, J. D., Nielsen, L. B., Jorgensen, S., Kjaergaard, H. G., and Wennberg, P. O.: Autoxidation of organic compounds in the atmosphere, J. Phys. Chem. Lett., 4, 3513-3520, 2013.

DeCarlo, P. F., Kimmel, J. R., Trimborn, A., Northway, M. J., Jayne, J. T., Aiken, A. C., Gonin, M., Fuhrer, K., Horvath, T., Docherty, K. S., Worsnop, D. R., and Jimenez, J. L.: Field-deployable, high-resolution, time-of-flight aerosol mass spectrometer, Anal. Chem., 78, 8281-8289, 2006.

DePalma, J. W., Horan, A. J., Hall, W. A., and Johnston, M. V.: Thermodynamics of oligomer formation: implications for secondary organic aerosol formation and reactivity, Phys. Chem. Chem. Phys., 15, 6935-6944, 2013.

Ding, X., He, Q. F., Shen, R. Q., Yu, Q. Q., and Wang, X. M.: Spatial distributions of secondary organic aerosols from isoprene, monoterpenes, beta-caryophyllene, and aromatics over China during summer, J. Geophys. Res., 119, 11877-11891, Doi 10.1002/2014jd021748, 2014.

Docherty, K. S., Wu, W., Lim, Y. B., and Ziemann, P. J.: Contributions of organic peroxides to secondary aerosol formed from reactions of monoterpenes with O_3, Environ. Sci. Technol., 39, 4049-4059, 2005.

Donahue, N. M., Drozd, G. T., Epstein, S. A., Presto, A. A., and Kroll, J. H.: Adventures in ozoneland: down the rabbit-hole, Phys. Chem. Chem. Phys., 13, 10848-10857, doi:10.1039/c0cp02564j, 2011.

Donahue, N. M., Ortega, I. K., Chuang, W., Riipinen, I., Riccobono, F., Schobesberger, S., Dommen, J., Baltensperger, U., Kulmala, M., Worsnop, D. R., and Vehkamaki, H.: How do organic vapors contribute to new-particle formation?, Faraday Discuss., 165, 91-104, doi:10.1039/c3fd00046j, 2013.

Duhl, T. R., Helmig, D., and Guenther, A.: Sesquiterpene emissions from vegetation: a review, Biogeosciences, 5, 761-777, 2008.

Ehn, M., Thornton, J. A., Kleist, E., Sipila, M., Junninen, H., Pullinen, I., Springer, M., Rubach, F., Tillmann, R., Lee, B., Lopez-Hilfiker, F., Andres, S., Acir, I. H., Rissanen, M., Jokinen, T., Schobesberger, S., Kangasluoma, J., Kontkanen, J., Nieminen, T., Kurten, T., Nielsen, L. B., Jorgensen, S., Kjaergaard, H. G., Canagaratna, M., Dal Maso, M., Berndt, T., Petaja, T., Wahner, A., Kerminen, V. M., Kulmala, M., Worsnop, D. R., Wildt, J., and Mentel, T. F.: A large source of low-volatility secondary organic aerosol, Nature, 506, 476-479, 2014.

Finlayson-Pitts, B. J., and Pitts, J. N.: Chemistry of the upper and lower atmosphere: theory, experiments, and applications, Academic Press, San Diego, 2000.

Gao, Y. Q., Hall, W. A., and Johnston, M. V.: Molecular composition of monoterpene secondary organic aerosol at low mss loading, Environ. Sci. Technol., 44, 7897-7902, doi:10.1021/Es101861k, 2010.

Goldstein, A. H., and Galbally, I. E.: Known and unexplored organic constituents in the earth's atmosphere, Environ. Sci. Technol., 41, 1514-1521, doi:10.1021/Es072476p, 2007.

Greaves, J., and Roboz, J.: Mass spectrometry for the novice, CRC Press, Boca Raton, F. L., USA, 2013.

Guenther, A., Hewitt, C. N., Erickson, D., Fall, R., Geron, C., Graedel, T., Harley, P., Klinger, L., Lerdau, M., Mckay, W. A., Pierce, T., Scholes, B., Steinbrecher, R., Tallamraju, R., Taylor, J., and Zimmerman, P.: A global-model of natural volatile organic compound emissions, J. Geophys. Res., 100, 8873-8892, doi:10.1029/94jd02950, 1995.

Hall, W. A., and Johnston, M. V.: Oligomer formation pathways in secondary organic aerosol from MS and MS/MS measurements with high mass accuracy and resolving power, J. Am. Soc. Mass Spectrom., 23, 1097-1108, 2012.

Hallquist, M., Wenger, J. C., Baltensperger, U., Rudich, Y., Simpson, D., Claeys, M., Dommen, J., Donahue, N. M., George, C., Goldstein, A. H., Hamilton, J. F., Herrmann, H., Hoffmann, T., Iinuma, Y., Jang, M., Jenkin, M. E., Jimenez, J. L., Kiendler-Scharr, A., Maenhaut, W., McFiggans, G., Mentel, T. F., Monod, A., Prevot, A. S. H., Seinfeld, J. H., Surratt, J. D., Szmigielski, R., and Wildt, J.: The formation, properties and impact of secondary organic aerosol: current and emerging issues, Atmos. Chem. Phys., 9, 5155-5236, 2009.

Harrick, N. J.: Internal reflection spectroscopy, Interscience Publishers, New York, 1967.

Heaton, K. J., Sleighter, R. L., Hatcher, P. G., Hall, W. A., and Johnston, M. V.: Composition domains in monoterpene secondary organic aerosol, Environ. Sci. Technol., 43, 7797-7802, 2009.

Helmig, D., Ortega, J., Duhl, T., Tanner, D., Guenther, A., Harley, P., Wiedinmyer, C., Milford, J., and Sakulyanontvittaya, T.: Sesquiterpene emissions from pine trees - Identifications, emission rates and flux estimates for the contiguous United States, Environ. Sci. Technol., 41, 1545-1553, doi:10.1021/Es0618907, 2007.

Hodas, N., Zuend, A., Mui, W., Flagan, R. C., and Seinfeld, J. H.: Influence of particle-phase state on the hygroscopic behavior of mixed organic-inorganic aerosols, Atmos. Chem. Phys., 15, 5027-5045, doi:10.5194/acp-15-5027-2015, 2015.

Hoffmann, T., Odum, J. R., Bowman, F., Collins, D., Klockow, D., Flagan, R. C., and Seinfeld, J. H.: Formation of organic aerosols from the oxidation of biogenic hydrocarbons, J. Atmos. Chem., 26, 189-222, doi:10.1023/A:1005734301837, 1997.

Hoffmann, T., Bandur, R., Marggraf, U., and Linscheid, M.: Molecular composition of organic aerosols formed in the alpha-pinene/O_3 reaction: Implications for new particle formation processes, J. Geophys. Res., 103, 25569-25578, 1998.

Hu, D., Bian, Q., Li, T. W. Y., Lau, A. K. H., and Yu, J. Z.: Contributions of isoprene, monoterpenes, beta-caryophyllene, and toluene to secondary organic aerosols in Hong Kong during the summer of 2006, J. Geophys. Res., 113, D22206, doi:10.1029/2008jd010437, 2008.

IPCC: Summary for Policymakers. In: Climate Change 2013: The Physical Science Basis. Contribution of Working Group I to the Fifth Assessment Report of the Intergovernmental Panel on Climate Change [Stocker, T.F., D. Qin, G.-K. Plattner, M. Tignor, S.K. Allen, J. Boschung, A. Nauels, Y. Xia, V. Bex and P.M. Midgley (eds.)]. Cambridge University Press, Cambridge, United Kingdom and New York, NY, USA., 2013.

Jaoui, M., Sexton, K. G., and Kamens, R. M.: Reaction of alpha-cedrene with ozone: mechanism, gas and particulate products distribution, Atmos. Environ., 38, 2709-2725, 2004.

Jaoui, M., Kleindienst, T. E., Docherty, K. S., Lewandowski, M., and Offenberg, J. H.: Secondary organic aerosol formation from the oxidation of a series of sesquiterpenes: alpha-cedrene, beta-caryophyllene, alpha-humulene and alpha-farnesene with O_3, OH and NO_3 radicals, Environ. Chem., 10, 178-193, doi:10.1071/En13025, 2013.

Jokinen, T., Berndt, T., Makkonen, R., Kerminen, V. M., Junninen, H., Paasonen, P., Stratmann, F., Herrmann, H., Guenther, A. B., Worsnop, D. R., Kulmala, M., Ehn, M., and Sipila, M.: Production of extremely low volatile organic compounds from biogenic emissions: Measured yields and atmospheric implications, Proc. Natl. Acad. Sci. U. S. A., 112, 7123-7128, doi:10.1073/pnas.1423977112, 2015.

Kanakidou, M., Seinfeld, J. H., Pandis, S. N., Barnes, I., Dentener, F. J., Facchini, M. C., Van Dingenen, R., Ervens, B., Nenes, A., Nielsen, C. J., Swietlicki, E., Putaud, J. P., Balkanski, Y., Fuzzi, S., Horth, J., Moortgat, G. K., Winterhalter, R., Myhre, C. E. L., Tsigaridis, K., Vignati, E., Stephanou, E. G., and Wilson, J.: Organic aerosol and global climate modelling: a review, Atmos. Chem. Phys., 5, 1053-1123, 2005.

Kanawati, B., Herrmann, F., Joniec, S., Winterhalter, R., and Moortgat, G. K.: Mass spectrometric characterization of beta-caryophyllene ozonolysis products in the aerosol studied using an electrospray triple quadrupole and time-of-flight analyzer hybrid system and density functional theory, Rapid Commun. Mass Spectrom., 22, 165-186, doi:10.1002/Rcm.3340, 2008.

Kidd, C., Perraud, V., and Finlayson-Pitts, B. J.: New insights into secondary organic aerosol from the ozonolysis of alpha-pinene from combined infrared spectroscopy and mass spectrometry measurements, Phys. Chem. Chem. Phys., 16, 22706-22716, 2014a.

Kidd, C., Perraud, V., Wingen, L. M., and Finlayson-Pitts, B. J.: Integrating phase and composition of secondary organic aerosol from the ozonolysis of alpha-pinene, Proc. Natl. Acad. Sci. U. S. A., 111, 7552-7557, 2014b.

Kim, H., Liu, S., Russell, L. M., and Paulson, S. E.: Dependence of real refractive indices on

O:C, H:C and mass fragments of secondary organic aerosol generated from ozonolysis and photooxidation of limonene and alpha-pinene, Aerosol Sci. Technol., 48, 498-507, doi:10.1080/02786826.2014.893278, 2014.

Koop, T., Bookhold, J., Shiraiwa, M., and Poschl, U.: Glass transition and phase state of organic compounds: dependency on molecular properties and implications for secondary organic aerosols in the atmosphere, Phys. Chem. Chem. Phys., 13, 19238-19255, 2011.

Kristensen, K., Enggrob, K. L., King, S. M., Worton, D. R., Platt, S. M., Mortensen, R., Rosenoern, T., Surratt, J. D., Bilde, M., Goldstein, A. H., and Glasius, M.: Formation and occurrence of dimer esters of pinene oxidation products in atmospheric aerosols, Atmos. Chem. Phys., 13, 3763-3776, 2013.

Kristensen, K., Cui, T., Zhang, H., Gold, A., Glasius, M., and Surratt, J. D.: Dimers in alpha-pinene secondary organic aerosol: effect of hydroxyl radical, ozone, relative humidity and aerosol acidity, Atmos. Chem. Phys., 14, 4201-4218, 2014.

Kroll, J. H., and Seinfeld, J. H.: Chemistry of secondary organic aerosol: Formation and evolution of low-volatility organics in the atmosphere, Atmos. Environ., 42, 3593-3624, 2008.

Lambe, A. T., Cappa, C. D., Massoli, P., Onasch, T. B., Forestieri, S. D., Martin, A. T., Cummings, M. J., Croasdale, D. R., Brune, W. H., Worsnop, D. R., and Davidovits, P.: Relationship between oxidation level and optical properties of secondary organic aerosol, Environ. Sci. Technol., 47, 6349-6357, 2013.

Lee, A., Goldstein, A. H., Keywood, M. D., Gao, S., Varutbangkul, V., Bahreini, R., Ng, N. L., Flagan, R. C., and Seinfeld, J. H.: Gas-phase products and secondary aerosol yields from the ozonolysis of ten different terpenes, J. Geophys. Res., 111, D07302, 10.1029/2005JD006437, 2006.

Lee, C. T., and Kamens, R. M.: Particle nucleation from the reaction of α–pinene and O_3, Atmos. Env., 39, 6822-6832, 2005.

Lewis, T. R., Blitz, M. A., Heard, D. E., and Seakins, P. W.: Direct evidence for a substantive reaction between the Criegee intermediate, CH_2OO, and the water vapour dimer, Phys. Chem. Chem. Phys., 17, 4859-4863, doi:10.1039/c4cp04750h, 2015.

Li, Y. J., Chen, Q., Guzman, M. I., Chan, C. K., and Martin, S. T.: Second-generation products contribute substantially to the particle-phase organic material produced by beta-caryophyllene ozonolysis, Atmos. Chem. Phys., 11, 121-132, doi:10.5194/acp-11-121-2011, 2011.

Lignell, H., Hinks, M. L., and Nizkorodov, S. A.: Exploring matrix effects on photochemistry of organic aerosols, Proc. Natl. Acad. Sci. U. S. A., 111, 13780-13785, 2014.

Mauderly, J. L., and Chow, J. C.: Health effects of organic aerosols, Inhalation Toxicol., 20, 257-288, doi:10.1080/08958370701866008, 2008.

Mehrer, H.: Diffusion in solids: fundamentals, methods, materials, diffusion-controlled processes, Springer series in solid state science, 155, Springer, Berlin; New York, 2007.

Mikhailov, E., Vlasenko, S., Martin, S. T., Koop, T., and Poschl, U.: Amorphous and crystalline aerosol particles interacting with water vapor: conceptual framework and experimental evidence for restructuring, phase transitions and kinetic limitations, Atmos. Chem. Phys., 9, 9491-9522, 2009.

Muller, L., Reinnig, M. C., Warnke, J., and Hoffmann, T.: Unambiguous identification of esters as oligomers in secondary organic aerosol formed from cyclohexene and cyclohexene/alpha-pinene ozonolysis, Atmos. Chem. Phys., 8, 1423-1433, 2008.

Muller, L., Reinnig, M. C., Hayen, H., and Hoffmann, T.: Characterization of oligomeric compounds in secondary organic aerosol using liquid chromatography coupled to electrospray ionization Fourier transform ion cyclotron resonance mass spectrometry, Rapid Commun. Mass Spectrom., 23, 971-979, 2009.

Nah, T., Chan, M., Leone, S. R., and Wilson, K. R.: Real time in situ chemical characterization of submicrometer organic particles using direct analysis in real time-mass spectrometry, Anal. Chem., 85, 2087-2095, doi:10.1021/ac302560c, 2013.

Ng, N. L., Kroll, J. H., Keywood, M. D., Bahreini, R., Varutbangkul, V., Flagan, R. C., Seinfeld, J. H., Lee, A., and Goldstein, A. H.: Contribution of first- versus second-generation products to secondary organic aerosols formed in the oxidation of biogenic hydrocarbons, Environ. Sci. Technol., 40, 2283-2297, doi:10.1021/Es052269u, 2006.

Pajunoja, A., Lambe, A. T., Hakala, J., Rastak, N., Cummings, M. J., Brogan, J. F., Hao, L. Q., Paramonov, M., Hong, J., Prisle, N. L., Malila, J., Romakkaniemi, S., Lehtinen, K. E. J., Laaksonen, A., Kulmala, M., Massoli, P., Onasch, T. B., Donahue, N. M., Riipinen, I., Davidovits, P., Worsnop, D. R., Petaja, T., and Virtanen, A.: Adsorptive uptake of water by semisolid secondary organic aerosols, Geophys. Res. Lett., 42, 3063-3068, doi:10.1002/2015GL063142, 2015.

Pankow, J. F., and Asher, W. E.: SIMPOL.1: a simple group contribution method for predicting vapor pressures and enthalpies of vaporization of multifunctional organic compounds, Atmos. Chem. Phys., 8, 2773-2796, 2008.

Perraud, V., Bruns, E. A., Ezell, M. J., Johnson, S. N., Yu, Y., Alexander, M. L., Zelenyuk, A., Imre, D., Chang, W. L., Dabdub, D., Pankow, J. F., and Finlayson-Pitts, B. J.: Nonequilibrium atmospheric secondary organic aerosol formation and growth, Proc. Natl. Acad. Sci. U. S. A., 109, 2836-2841, 2012.

Reinnig, M. C., Warnke, J., and Hoffmann, T.: Identification of organic hydroperoxides and hydroperoxy acids in secondary organic aerosol formed during the ozonolysis of different monoterpenes and sesquiterpenes by on-line analysis using atmospheric pressure chemical ionization ion trap mass spectrometry, Rapid Commun. Mass Spectrom., 23, 1735-1741, doi:10.1002/Rcm.4065, 2009.

Renbaum-Wolff, L., Grayson, J. W., Bateman, A. P., Kuwata, M., Sellier, M., Murray, B. J., Shilling, J. E., Martin, S. T., and Bertram, A. K.: Viscosity of alpha-pinene secondary organic material and implications for particle growth and reactivity, Proc. Natl. Acad. Sci. U. S. A., 110, 8014-8019, 2013.

Renbaum, L. H., and Smith, G. D.: The importance of phase in the radical-initiated oxidation of model organic aerosols: reactions of solid and liquid brassidic acid particles, Phys. Chem. Chem. Phys., 11, 2441-2451, doi:10.1039/b816799k, 2009.

Richters, S., Herrmann, H., and Berndt, T.: Gas-phase rate coefficients of the reaction of ozone with four sesquiterpenes at 295 +/- 2 K, Phys. Chem. Chem. Phys., 17, 11658-11669, doi:10.1039/c4cp05542j, 2015.

Riipinen, I., Pierce, J. R., Yli-Juuti, T., Nieminen, T., Hakkinen, S., Ehn, M., Junninen, H., Lehtipalo, K., Petaja, T., Slowik, J., Chang, R., Shantz, N. C., Abbatt, J., Leaitch, W. R., Kerminen, V. M., Worsnop, D. R., Pandis, S. N., Donahue, N. M., and Kulmala, M.: Organic condensation: a vital link connecting aerosol formation to cloud condensation nuclei (CCN) concentrations, Atmos. Chem. Phys., 11, 3865-3878, doi:10.5194/acp-11-3865-2011, 2011.

Rissanen, M. P., Kurten, T., Sipila, M., Thornton, J. A., Kausiala, O., Garmash, O., Kjaergaard, H.

G., Petaja, T., Worsnop, D. R., Ehn, M., and Kulmala, M.: Effects of chemical complexity on the autoxidation mechanisms of endocyclic alkene ozonolysis products: from methylcyclohexenes toward understanding alpha-pinene, J. Phys. Chem. A, 119, 4633-4650, doi:10.1021/jp510966g, 2015.

Ruscic, B.: Active thermochemical tables: water and water dimer, J. Phys. Chem. A, 117, 11940-11953, doi:10.1021/jp403197t, 2013.

Ryzhkov, A. B., and Ariya, P. A.: A theoretical study of the reactions of parent and substituted Criegee intermediates with water and the water dimer, Phys. Chem. Chem. Phys., 6, 5042-5050, doi:10.1039/b408414d, 2004.

Sadezky, A., Winterhalter, R., Kanawati, B., Rompp, A., Spengler, B., Mellouki, A., Le Bras, G., Chaimbault, P., and Moortgat, G. K.: Oligomer formation during gas-phase ozonolysis of small alkenes and enol ethers: new evidence for the central role of the Criegee Intermediate as oligomer chain unit, Atmos. Chem. Phys., 8, 2667-2699, 2008.

Sakulyanontvittaya, T., Duhl, T., Wiedinmyer, C., Helmig, D., Matsunaga, S., Potosnak, M., Milford, J., and Guenther, A.: Monoterpene and sesquiterpene emission estimates for the United States, Environ. Sci. Technol., 42, 1623-1629, doi:10.1021/Es702274e, 2008a.

Sakulyanontvittaya, T., Guenther, A., Helmig, D., Milford, J., and Wiedinmyer, C.: Secondary organic aerosol from sesquiterpene and monoterpene emissions in the United States, Environ. Sci. Technol., 42, 8784-8790, doi:10.1021/Es800817r, 2008b.

Saukko, E., Lambe, A. T., Massoli, P., Koop, T., Wright, J. P., Croasdale, D. R., Pedernera, D. A., Onasch, T. B., Laaksonen, A., Davidovits, P., Worsnop, D. R., and Virtanen, A.: Humidity-dependent phase state of SOA particles from biogenic and anthropogenic precursors, Atmos. Chem. Phys., 12, 7517-7529, doi:10.5194/acp-12-7517-2012, 2012.

Seinfeld, J. H., and Pandis, S. N.: Atmospheric chemistry and physics: from air pollution to climate change, 2nd ed., J. Wiley, Hoboken, N.J., 2006.

Shiraiwa, M., Ammann, M., Koop, T., and Poschl, U.: Gas uptake and chemical aging of semisolid organic aerosol particles, Proc. Natl. Acad. Sci. U. S. A., 108, 11003-11008, 2011.

Shiraiwa, M., and Seinfeld, J. H.: Equilibration timescale of atmospheric secondary organic aerosol partitioning, Geophys. Res. Lett., 39, L24801, doi:10.1029/2012GL054008, 2012.

Shiraiwa, M., Selzle, K., and Poschl, U.: Hazardous components and health effects of atmospheric aerosol particles: reactive oxygen species, soot, polycyclic aromatic compounds and allergenic proteins, Free Radical Res., 46, 927-939, doi:10.3109/10715762.2012.663084, 2012.

Shu, Y. G., and Atkinson, R.: Rate constants for the gas-phase reactions of O_3 with a series of terpenes and OH radical formation from the O_3 reactions with sesquiterpenes at 296+/-2 K, Int. J. Chem. Kinet., 26, 1193-1205, 1994.

Slade, J. H., and Knopf, D. A.: Multiphase OH oxidation kinetics of organic aerosol: The role of particle phase state and relative humidity, Geophys. Res. Lett., 41, 5297-5306, doi:10.1002/2014GL060582, 2014.

Socrates, G.: Infrared and Raman characteristic group frequencies: tables and charts, 3rd ed., Wiley, Chichester; New York, 2001.

Taatjes, C. A., Welz, O., Eskola, A. J., Savee, J. D., Scheer, A. M., Shallcross, D. E., Rotavera, B., Lee, E. P. F., Dyke, J. M., Mok, D. K. W., Osborn, D. L., and Percival, C. J.: Direct measurements of conformer-dependent reactivity of the criegee intermediate CH_3CHOO, Science, 340, 177-180, 2013.

Tasoglou, A., and Pandis, S. N.: Formation and chemical aging of secondary organic aerosol during the beta-caryophyllene oxidation, Atmos. Chem. Phys., 15, 6035-6046, doi:10.5194/acp-15-6035-2015, 2015.

Tolocka, M. P., Jang, M., Ginter, J. M., Cox, F. J., Kamens, R. M., and Johnston, M. V.: Formation of oligomers in secondary organic aerosol, Environ. Sci. Technol., 38, 1428-1434, 2004.

Vaden, T. D., Imre, D., Beranek, J., Shrivastava, M., and Zelenyuk, A.: Evaporation kinetics and phase of laboratory and ambient secondary organic aerosol, Proc. Natl. Acad. Sci. U. S. A., 108, 2190-2195, 2011.

Vereecken, L., Muller, J. F., and Peeters, J.: Low-volatility poly-oxygenates in the OH-initiated atmospheric oxidation of alpha-pinene: impact of non-traditional peroxyl radical chemistry, Phys. Chem. Chem. Phys., 9, 5241-5248, 2007.

Vereecken, L., Harder, H., and Novelli, A.: The reaction of Criegee intermediates with NO, RO_2, and SO_2, and their fate in the atmosphere, Phys. Chem. Chem. Phys., 14, 14682-14695, 2012.

Virtanen, A., Joutsensaari, J., Koop, T., Kannosto, J., Yli-Pirila, P., Leskinen, J., Makela, J. M., Holopainen, J. K., Poschl, U., Kulmala, M., Worsnop, D. R., and Laaksonen, A.: An amorphous solid state of biogenic secondary organic aerosol particles, Nature, 467, 824-827, doi:10.1038/nature09455, 2010.

Welz, O., Eskola, A. J., Sheps, L., Rotavera, B., Savee, J. D., Scheer, A. M., Osborn, D. L., Lowe, D., Booth, A. M., Xiao, P., Khan, M. A. H., Percival, C. J., Shallcross, D. E., and Taatjes, C. A.: Rate coefficients of C1 and C2 Criegee intermediate reactions with formic and acetic acid near the collision limit: direct kinetics measurements and atmospheric implications, Angew. Chem.-Int. Ed., 53, 4547-4550, 2014.

Winkler, P. M., Ortega, J., Karl, T., Cappellin, L., Friedli, H. R., Barsanti, K., McMurry, P. H., and Smith, J. N.: Identification of the biogenic compounds responsible for size-dependent nanoparticle growth, Geophys. Res. Lett., 39, L20815, doi:10.1029/2012gl053253, 2012.

Winterhalter, R., Herrmann, F., Kanawati, B., Nguyen, T. L., Peeters, J., Vereecken, L., and Moortgat, G. K.: The gas-phase ozonolysis of beta-caryophyllene ($C_{15}H_{24}$). Part I: an experimental study, Phys. Chem. Chem. Phys., 11, 4152-4172, doi:10.1039/B817824k, 2009.

Witkowski, B., and Gierczak, T.: Analysis of alpha-acyloxyhydroperoxy aldehydes with electrospray ionization-tandem mass spectrometry (ESI-MS^n), J. Mass Spectrom., 48, 79-88, doi:10.1002/jms.3130, 2013.

Witkowski, B., and Gierczak, T.: Early stage composition of SOA produced by alpha-pinene/ozone reaction: alpha-Acyloxyhydroperoxy aldehydes and acidic dimers, Atmos. Environ., 95, 59-70, 2014.

Yao, L., Ma, Y., Wang, L., Zheng, J., Khalizov, A., Chen, M. D., Zhou, Y. Y., Qi, L., and Cui, F. P.: Role of stabilized Criegee intermediate in secondary organic aerosol formation from the ozonolysis of alpha-cedrene, Atmos. Environ., 94, 448-457, 2014.

Yasmeen, F., Vermeylen, R., Szmigielski, R., Iinuma, Y., Boge, O., Herrmann, H., Maenhaut, W., and Claeys, M.: Terpenylic acid and related compounds: precursors for dimers in secondary organic aerosol from the ozonolysis of alpha- and beta-pinene, Atmos. Chem. Phys., 10, 9383-9392, 2010.

Ying, Q., Li, J. Y., and Kota S. H.: Significant contributions of isoprene to summertime secondary organic aerosol in eastern United States, Environ. Sci. Technol., 49, 7834−7842, 2015.

Zhang, Q., Jimenez, J. L., Canagaratna, M. R., Allan, J. D., Coe, H., Ulbrich, I., Alfarra, M. R., Takami, A., Middlebrook, A. M., Sun, Y. L., Dzepina, K., Dunlea, E., Docherty, K., DeCarlo, P. F., Salcedo, D., Onasch, T., Jayne, J. T., Miyoshi, T., Shimono, A., Hatakeyama, S., Takegawa, N., Kondo, Y., Schneider, J., Drewnick, F., Borrmann, S., Weimer, S., Demerjian, K., Williams, P., Bower, K., Bahreini, R., Cottrell, L., Griffin, R. J., Rautiainen, J., Sun, J. Y., Zhang, Y. M., and Worsnop, D. R.: Ubiquity and dominance of oxygenated species in organic aerosols in anthropogenically-influenced Northern Hemisphere midlatitudes, Geophys. Res. Lett., 34, L13801, doi:10.1029/2007gl029979, 2007.

Zhang, R. Y., Wang, G. H., Guo, S., Zarnora, M. L., Ying, Q., Lin, Y., Wang, W. G., Hu, M., and Wang, Y.: Formation of urban fine particulate matter, Chem. Rev., 115, 3803-3855, doi:10.1021/acs.chemrev.5b00067, 2015.

Zhang, X., McVay, R. C., Huang, D. D., Dalleska, N. F., Aumont, B., Flagan, R. C., and Seinfeld, J. H.: Formation and evolution of molecular products in α-pinene secondary organic aerosol, Proc. Natl. Acad. Sci. U. S. A., 112, 14168-14173, doi: 10.1073/pnas.1517742112, 2015.

Zhao, J., Ortega, J., Chen, M., McMurry, P. H., and Smith, J. N.: Dependence of particle nucleation and growth on high-molecular-weight gas-phase products during ozonolysis of α-pinene, Atmos. Chem. Phys., 13, 7631-7644, doi:10.5194/acp-13-7631-2013, 2013.

Zhao, Y., Wingen, L. M., Perraud, V., Greaves, J., and Finlayson-Pitts, B. J.: Role of the reaction of stabilized Criegee intermediates with peroxy radicals in particle formation and growth in air, Phys. Chem. Chem. Phys., 17, 12500-12514, doi:10.1039/C5cp01171j, 2015.

Ziemann, P. J., and Atkinson, R.: Kinetics, products, and mechanisms of secondary organic aerosol formation, Chem. Soc. Rev., 41, 6582-6605, 2012.

Table 1 Summary of different types of flow reactor and chamber experiments

Exp type [a]	[VOC] (ppb)[b]	[O$_3$] (ppm)[c]	[HCOOH] or [2-EHN]	RH (%)	Reaction time	Particle size (nm)[d, e]	Particle mass conc. (µg m^{-3})[e]	Particle number conc. (10^6 cm^{-3}) [e]
^{2}FR1	138	14	none	< 1	27 s	15.2 ± 0.2	26 ± 2	7.9 ± 0.2
^{2}FR2	138	14	none	< 1	44 s	22.5 ± 0.8	71 ± 8	7.0 ± 0.2
^{2}FR3	63	16	none	< 1	30 s	13.1 ± 0.4	10 ± 1	5.3 ± 0.3
^{5}FR4	138	16	none	< 1	30 s	17.6 ± 0.9	52 ± 3	9.4 ± 0.3
^{2}FR5	275	16	none	< 1	30 s	25.7 ± 1.1	180 ± 16	11.8 ± 0.6
^{2}FR6	138	16	none	75	30 s	16.1 ± 0.9	36 ± 10	9.3 ± 1.7
^{2}FR7	138	16	2 ppm HCOOH	< 1	30 s	22.1 ± 0.4	41 ± 2	2.7 ± 0.1
^{2}FR8	138	16	15 ppm HCOOH	< 1	30 s	22.0 ± 0.8	25 ± 1	1.5 ± 0.1
^{4}CH1	34	1.5	none	< 5	30 min	66 ± 2	73 ± 6	0.34 ± 0.02
^{4}CH2	34	1.5	none	72	30 min	64 ± 2	66 ± 4	0.34 ± 0.03
^{3}CH3	1000	0.12	none	< 5	30 min	111 ± 1	363 ± 37	0.37 ± 0.03
^{3}CH4	215	1.5	none	< 5	60 min	140 ± 3	984 ± 186	0.40 ± 0.02
^{2}CH5	215	1.5	400 ppb 2-EHN	< 1	60 min	127 ± 5	663 ± 44	0.35 ± 0.02

[a] FR and CH represent flow reactor and chamber experiments, respectively. The numbers in front of the labels represent the times an experiment was repeated.

[b] The concentrations were calculated from the amount of α-cedrene liquid injected into the flow reactor and chamber, and the total gas flow.

[c] High O$_3$ concentration is needed to get enough reaction to form particles in less than a min in FR experments.

[d] Geometric mean diameter; the size distributions of SOA formed in the flow reactor are given in Figs. S1 and 11.

[e] All the data are given as "average value ± one standard deviation". SOA mass concentrations are obtained using a particle density of 1.1 g cm^{-3} (Yao et al., 2014). The chamber SOA data are given for 30 or 60 min reaction times, and were not corrected for the wall loss.

Table 2 Accurate mass and elemental formulae for P1 and P2 products formed from α-cedrene ozonolysis measured by ESI-ToF-MS.

Product[a]	ESI+ mode ([M+Na]$^+$)					ESI− mode ([M-H]$^-$)				
	Observed accurate mass (Da)	Elemental formula	Calculated exact mass (Da)	Absolute mass error (mDa)	Relative mass error (ppm)	Observed accurate mass (Da)	Elemental formula	Calculated exact mass (Da)	Absolute mass error (mDa)	Relative mass error (ppm)
P1-245	245.1525	$C_{14}H_{22}O_2Na$	245.1517	0.8	3.3	— [b]				
P1-247	247.1326	$C_{13}H_{20}O_3Na$	247.1310	1.6	6.4	223.1341	$C_{13}H_{19}O_3$	223.1334	0.7	3.1
P1-259	259.1681	$C_{15}H_{24}O_2Na$	259.1674	0.7	2.7	— [b]				
P1-261	— [b]					237.1494	$C_{14}H_{21}O_3$	237.1491	0.3	1.3
P1-275	275.1628	$C_{15}H_{24}O_3Na$	275.1623	0.5	1.8	251.1646	$C_{15}H_{23}O_3$	251.1647	-0.1	-0.4
P1-277	277.1422	$C_{14}H_{22}O_4Na$	277.1416	0.6	2.2	253.1447	$C_{14}H_{21}O_4$	253.1440	0.7	2.8
P1-289	289.1431	$C_{15}H_{22}O_4Na$	289.1416	1.5	5.2	265.1476	$C_{15}H_{21}O_4$	265.1440	3.6	13.6 [d]
P1-291	291.1577	$C_{15}H_{24}O_4Na$	291.1572	0.5	1.6	267.1607	$C_{15}H_{23}O_4$	267.1596	1.1	4.1
P1-305	305.1370	$C_{15}H_{22}O_5Na$	305.1365	0.5	1.7	— [b]				
P1-307	307.1516	$C_{15}H_{24}O_5Na$	307.1521	-0.5	-1.8	283.1554	$C_{15}H_{23}O_5$	283.1545	0.9	3.2
P1-321	321.1308	$C_{15}H_{22}O_6Na$	321.1314	-0.6	-1.9	297.1345	$C_{15}H_{21}O_6$	297.1338	0.7	2.4
P1-323	323.1465	$C_{15}H_{24}O_6Na$	323.1471	-0.6	-1.9	299.1492	$C_{15}H_{23}O_6$	299.1495	-0.3	-1.0
P2-481	481.3298	$C_{29}H_{46}O_4Na$	481.3294	0.4	0.8	— [b]				
P2-497	497.3262	$C_{29}H_{46}O_5Na$	497.3243	1.9	3.8	473.3271	$C_{29}H_{45}O_5$	473.3267	0.4	0.9
P2-511 [c]	511.3337	$C_{30}H_{48}O_5Na$	511.3399	-6.2	-12.1[d]	487.3086	$C_{29}H_{43}O_6$	487.3060	2.6	5.3
P2-513	513.3203	$C_{29}H_{46}O_6Na$	513.3192	1.1	2.1	489.3215	$C_{29}H_{45}O_6$	489.3216	-0.1	-0.2
P2-527	527.3317	$C_{30}H_{48}O_6Na$	527.3348	-3.1	-5.8	503.3387	$C_{30}H_{47}O_6$	503.3372	1.5	3.0
P2-543	543.3309	$C_{30}H_{48}O_7Na$	543.3298	1.1	2.0	519.3320	$C_{30}H_{47}O_7$	519.3322	-0.2	-0.4

[a] Labels “P1-xxx” and “P2-xxx” denote P1 and P2 products having a nominal mass of xxx for their sodiated ions, respectively.

[b] Accurate mass was not measured because of the very low ion intensity or the strong interference from other ions such as impurities.

[c] Different formulae for P2-511 were identified in ESI+ and ESI− modes, which correspond, respectively, to aldol condensation products (P2-511-3 and P2-511-4) and esters (P2-511-1 and P2-511-2) as shown in Fig. 10c.

[d] The relatively large mass errors likely result from unknown interferences for P1-289 in ESI− mode and P2-511 in ESI+ mode. The given formulae are the closest to the observed masses but may not be correct because of the interferences.

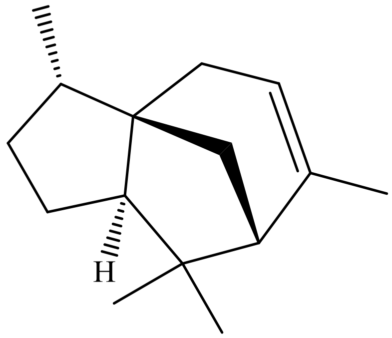

Figure 1 The structure of α-cedrene.

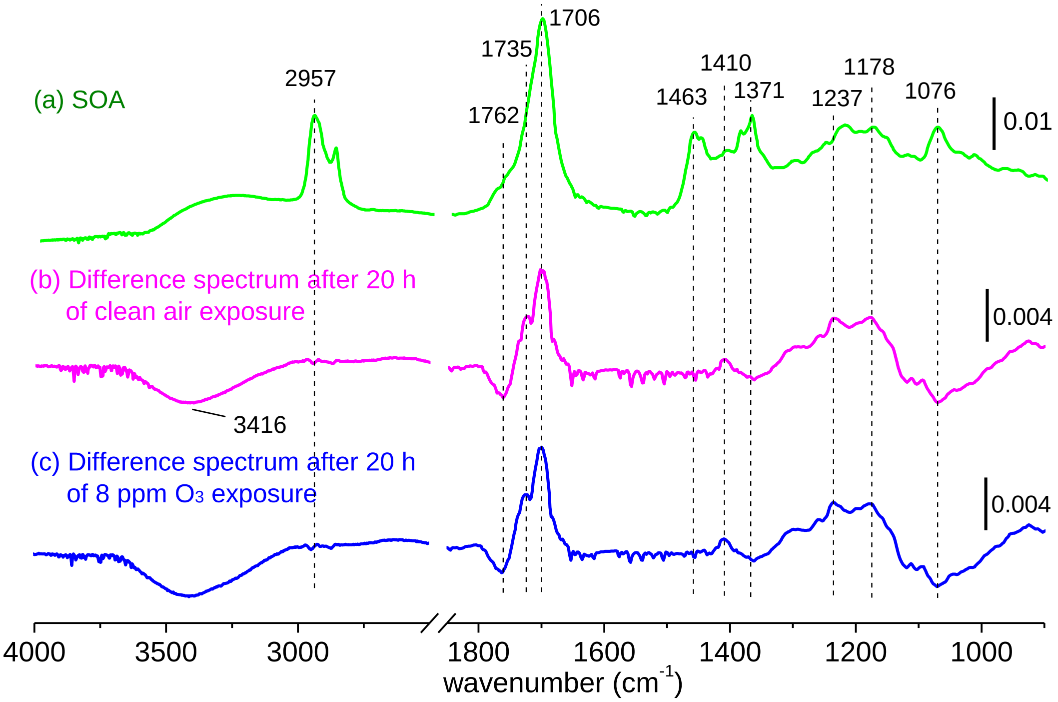

Figure 2 (a) A typical ATR-FTIR spectrum of SOA from ozonolysis of α-cedrene in the chamber (experiment CH4, Table1). This spectrum is obtained from $\log_{10}(S_0/S_1)$ where S_0 is the single beam spectrum of the clean crystal and S_1 is that of the SOA covered crystal recorded immediately following impaction. (b) and (c) Typical difference spectra of SOA after 20 hours of exposure to a flow of clean and 8 ppm O_3-containing dry air, respectively. These spectra are $\log_{10}(S_1/S_{20})$ where S_1 is the single beam spectrum of SOA covered crystal collected immediately following impaction and S_{20} is that after 20 hours of air or O_3 exposure. The positive and negative peaks in the difference spectra represent an increase and decrease, respectively, of the functional groups in SOA over 20 hours of exposure.

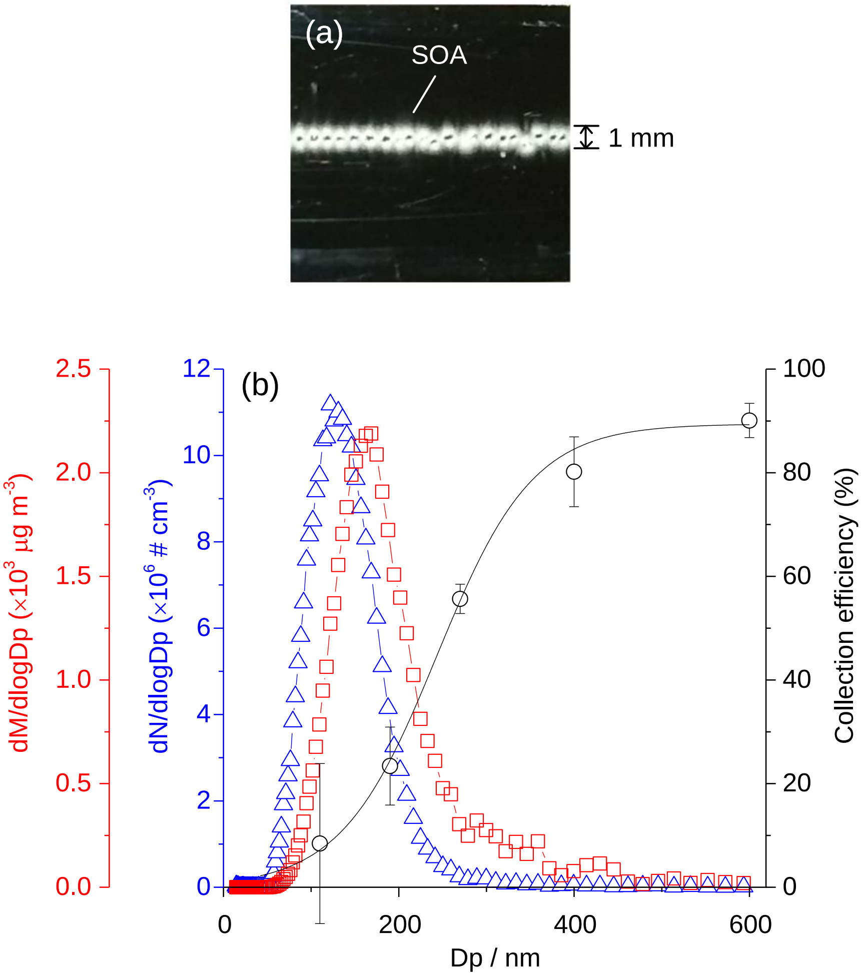

Figure 3 (a) Digital photograph of a typical impaction pattern of SOA formed by ozonolysis of α-cedrene in the presence of 2-EHN in the chamber (experiment CH5, Table 1). The photograph shows a 1 cm × 1 cm section of the crystal. The impacted SOA forms a narrow film ~1 mm in width along the centerline of the crystal. (b) The number (blue triangles) and mass (red squares) weighted size distribution of chamber α-cedrene SOA formed in the presence of 2-EHN. Also shown is the collection efficiency of the impactor as a function of particle diameter (black circle) measured using carboxylate-modified latex (CML) spheres in a previous study (Kidd et al., 2014b).

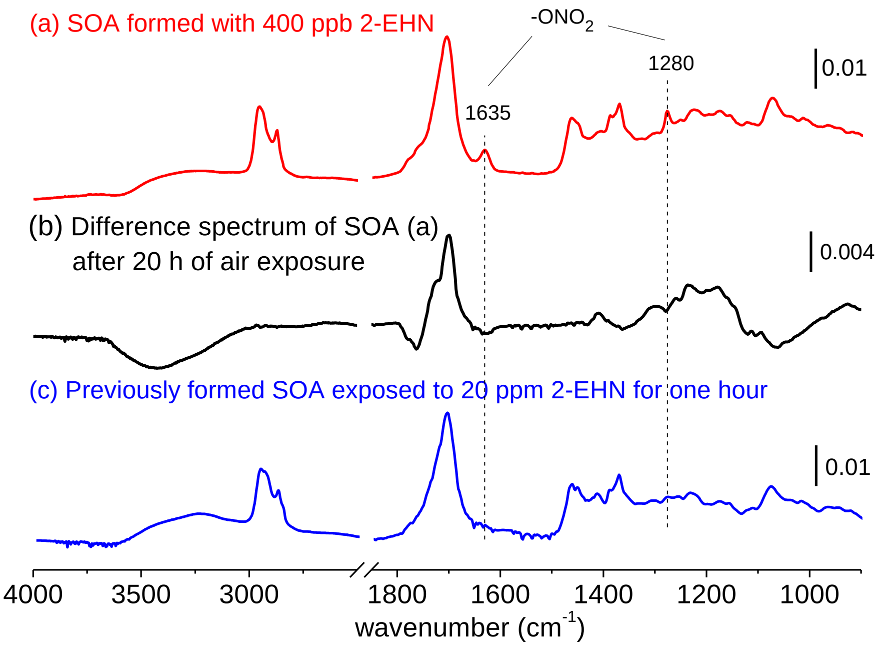

Figure 4 (a) A typical ATR-FTIR spectrum of SOA from ozonolysis of α-cedrene in the presence of gas phase 2-EHN in the chamber (experiment CH5, Table 1). This spectrum is obtained from $\log_{10}(S_0/S_1)$ where S_0 and S_1 are the single beam spectra of the clean crystal and SOA covered crystal recorded immediately following impaction. (b) A typical difference spectrum of SOA after 20 hours of exposure to a flow of clean dry air. This spectrum is $\log_{10}(S_1/S_{20})$ where S_1 and S_{20} are the single beam spectra of SOA covered crystal recorded immediately following impaction and after 20 hours of air exposure. The positive and negative peaks in the spectra represent an increase and decrease in the functional groups over 20 hours of air exposure, respectively. (c) ATR-FTIR spectrum of SOA formed without 2-EHN following exposure to a flow of dry air containing 20 ppm 2-EHN for one hour. This spectrum is derived from $\log_{10}(S_0/S_1)$ where S_0 and S_1 are the single beam spectra of the clean crystal and SOA covered crystal exposed to 20 ppm 2-EHN for one hour, respectively.

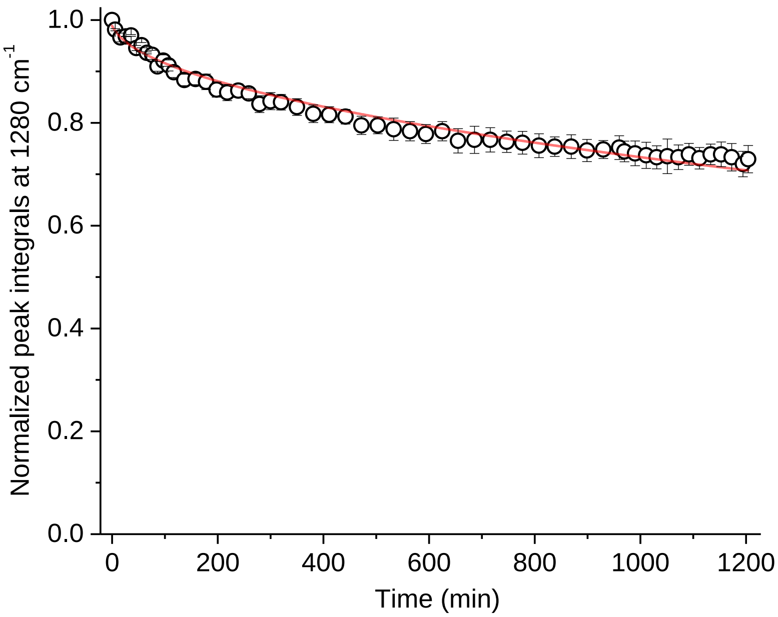

Figure 5 The normalized integrated area of –ONO_2 peak at 1280 cm^{-1} as a function of time over 20 hours of clean, dry air exposure. The red line is a best fit ($R^2 = 0.976$) of the evaporation data to eq. (1). Error bars represent ± 1 σ.

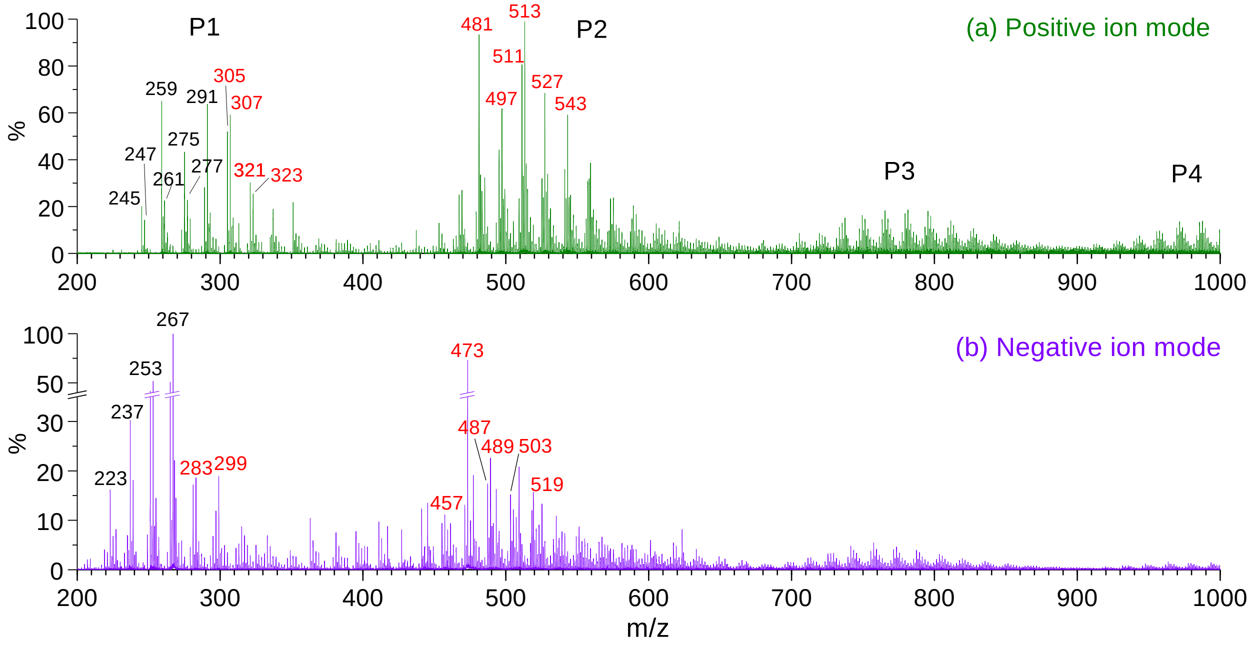

Figure 6 ESI mass spectra of SOA formed from ozonolysis of α-cedrene in the flow reactor (experiment FR4, Table1) in (a) positive and (b) negative ion modes. Black and red labels indicate the previously reported (Jaoui et al., 2004, 2013; Reinnig et al., 2009; Yao et al., 2014) and newly observed products, respectively. P1 represents the low molecular weight products, and P2, P3, and P4 denote higher molecular weight products formed by combinations of two, three, or four of the P1 products, respectively.

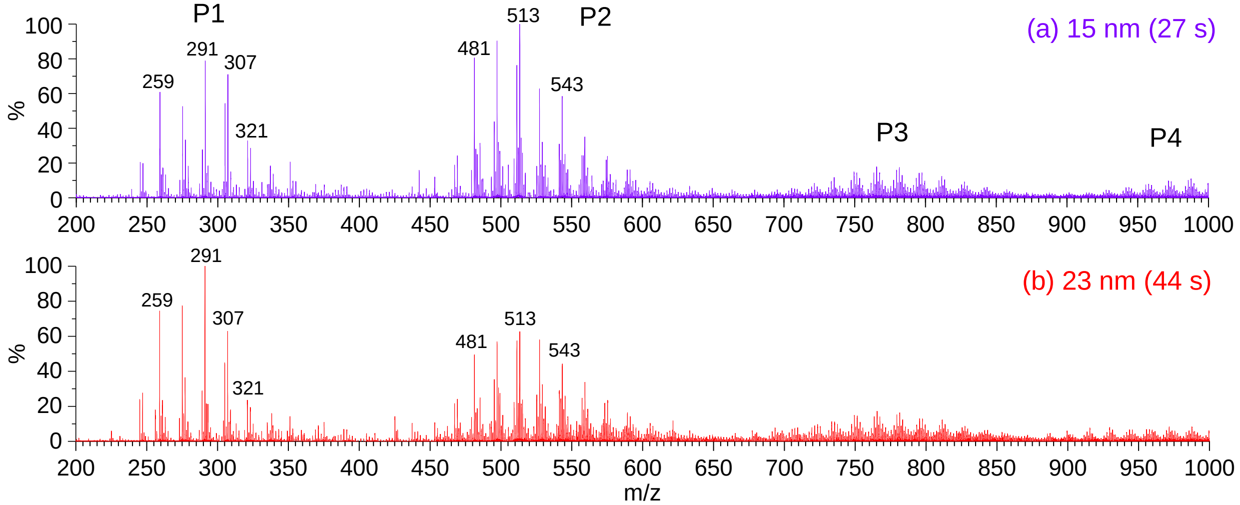

Figure 7 ESI (+) mass spectra of polydisperse SOA with geometric mean diameter of (a) 15 nm and (b) 23 nm formed from ozonolysis of α-cedrene in the flow reactor at 27 s and 44 s reaction times, respectively, under dry conditions (experiments FR1 and FR2, Table 1). The size distributions of SOA are shown in Fig. S1a. Note that these experiments were conducted as a separate series from other experiments. Because ESI-MS sensitivity changes over long periods (a month or more), the intensity ratios of oligomer to P1 products in the mass spectra shown here cannot be directly compared with other mass spectra obtained in this work. However, those ratios in the above mass spectra are comparable with each other as they were acquired on the timescale of days, over which ESI-MS sensitivity is essentially constant.

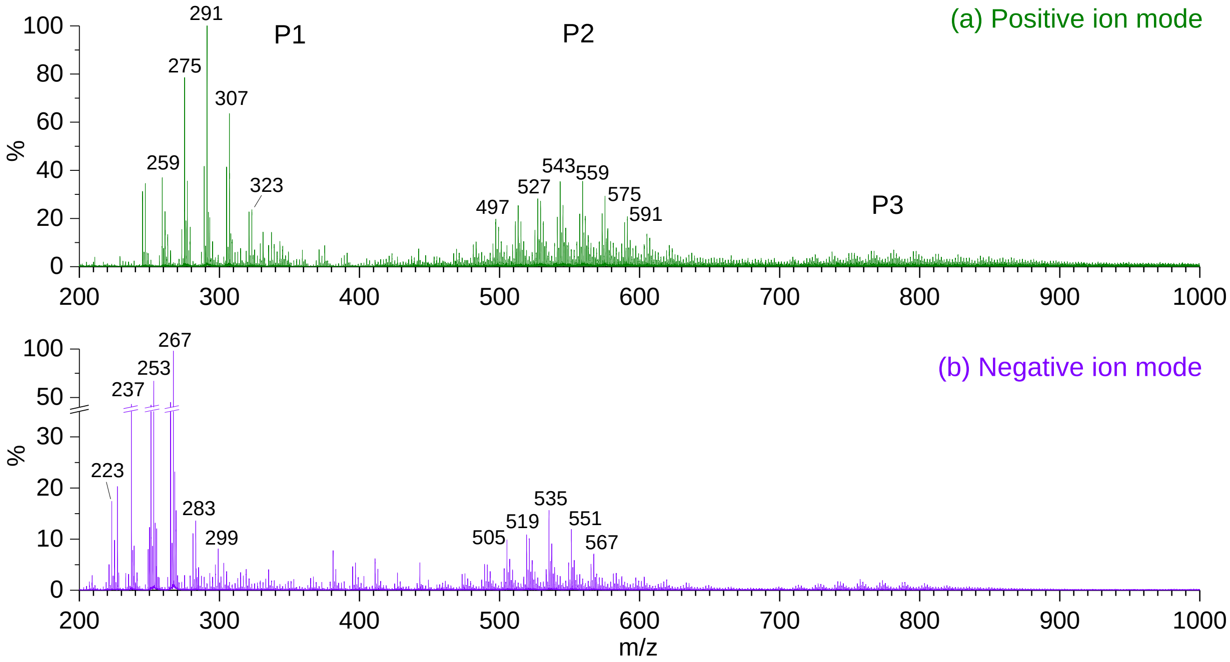

Figure 8 ESI mass spectra of SOA formed from ozonolysis of α-cedrene in the chamber (experiment CH1, Table 1) in (a) positive and (b) negative ion modes.

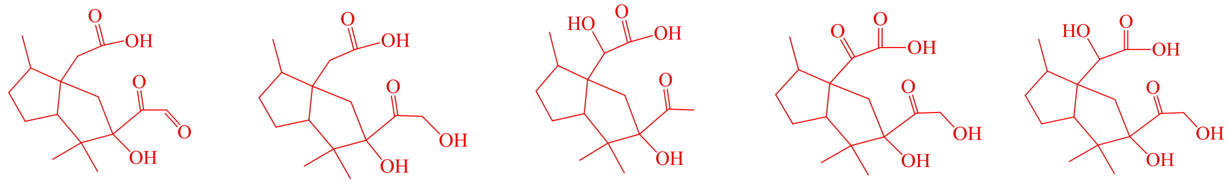

P1-305 (MW: 282) P1-307-1 (MW: 284) P1-307-2 (MW: 284) P1-321 (MW: 298) P1-323 (MW: 300)

Figure 9 The proposed potential structures of the newly observed products corresponding to the $[M+Na]^+$ ions of *m/z* 305, 307, 321, and 323. Label "P1-xxx" represents a P1 product, the sodiated ion of which has a nominal mass of xxx. Labels "P1-xxx-1" and "P1-xxx-2" indicate different isomeric structures for the product "P1-xxx". MW, molecular weight. Note that there may be additional isomeric structures for these products.

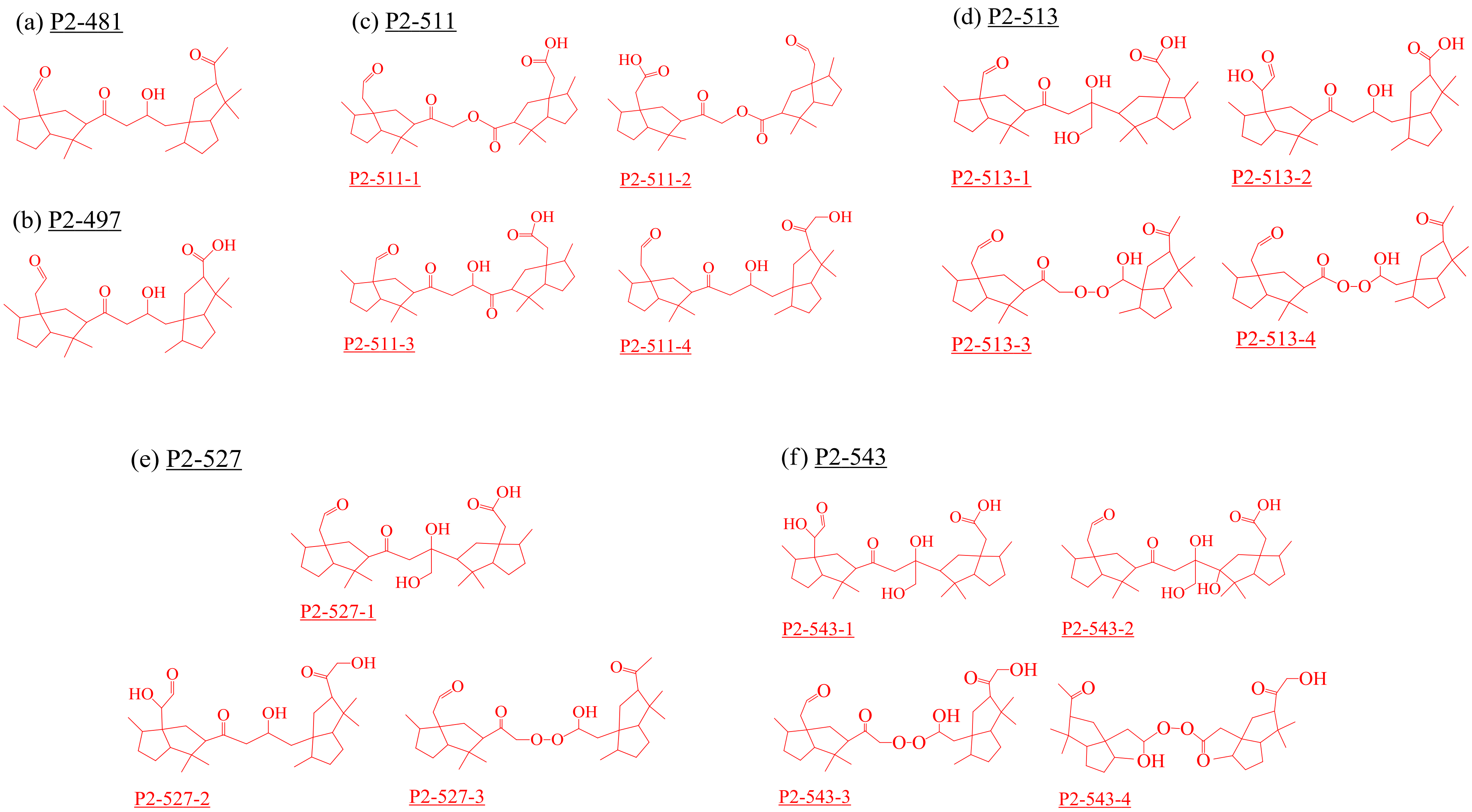

(a) P2-481

(b) P2-497

(c) P2-511

P2-511-1

P2-511-2

P2-511-3

P2-511-4

(d) P2-513

P2-513-1

P2-513-2

P2-513-3

P2-513-4

(e) P2-527

P2-527-1

P2-527-2

P2-527-3

(f) P2-543

P2-543-1

P2-543-2

P2-543-3

P2-543-4

Figure 10 The potential structures for the P2 products corresponding to the $[M+Na]^+$ ions of (a) *m/z* 481, (b) *m/z* 497, (c) *m/z* 511, (d) *m/z* 513, (e) *m/z* 527, and (f) *m/z* 543 formed from α-cedrene ozonolysis. Label "P2-xxx" represents a P2 product, the sodiated ion of which has a nominal mass of xxx. Label "P2-xxx-n" (n = 1-4) indicates different potential structures for the product "P2-xxx". Note that there may be additional isomeric structures for these products.

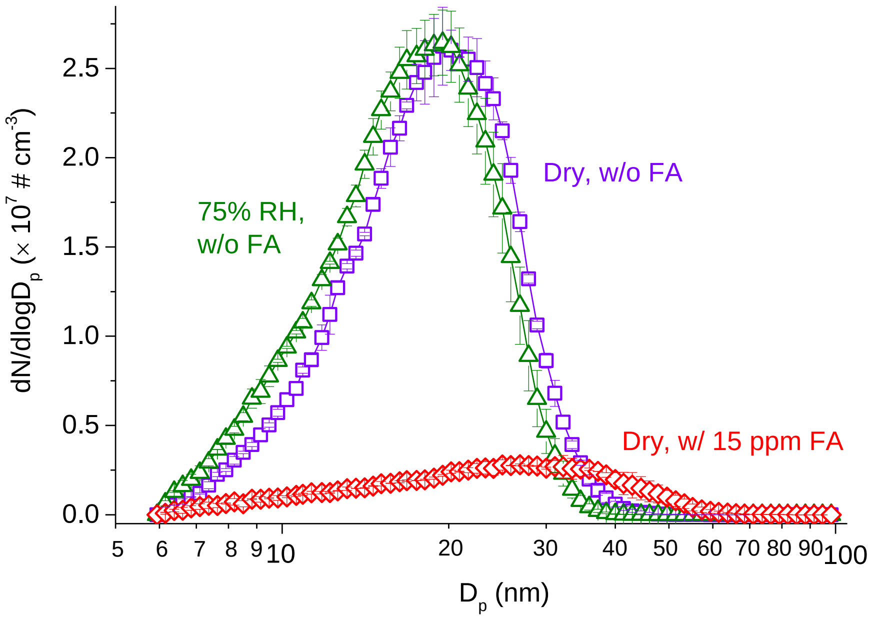

Figure 11 The size distributions of SOA formed from ozonolysis of α-cedrene in the flow reactor under dry conditions (purple squares, experiment FR4), at 75% RH (green triangles, experiment FR6), or in the presence of 15 ppm formic acid (red diamonds, experiment FR8).

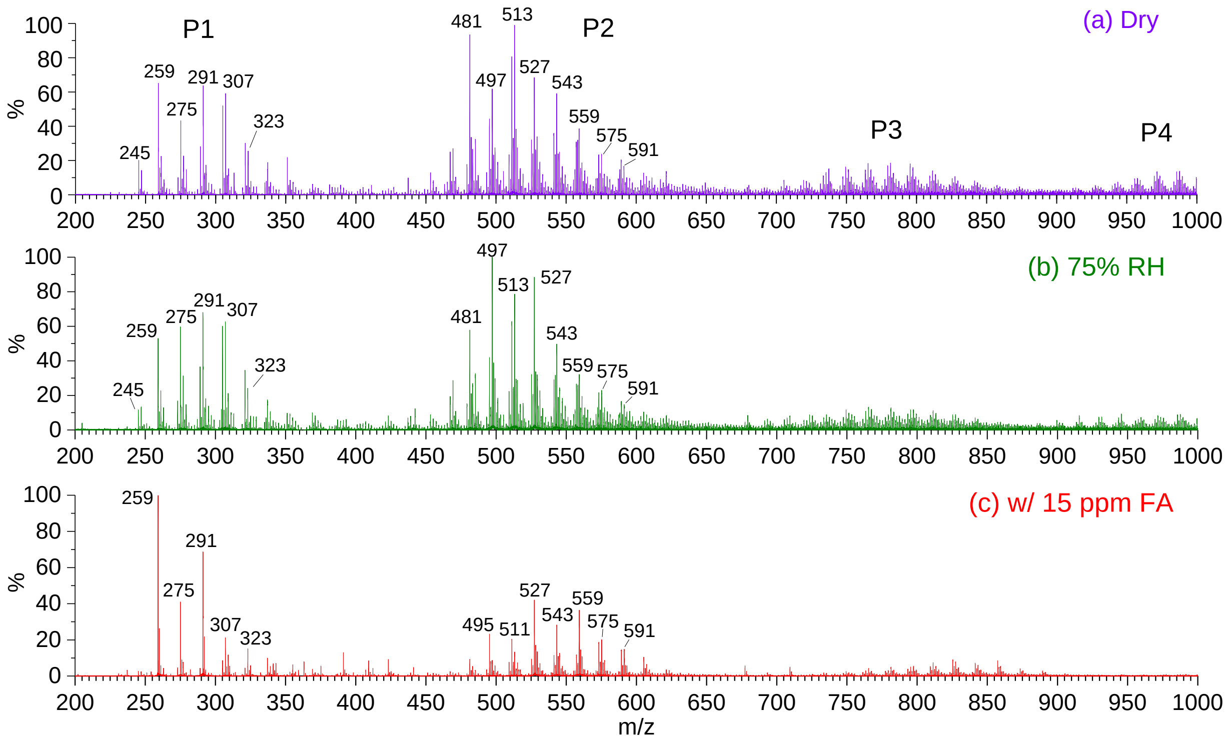

Figure 12 ESI (+) mass spectra of polydisperse SOA formed from ozonolysis of α-cedrene in the flow reactor (a) under dry conditions (experiment FR4), (b) at 75% RH (experiment FR6), and (c) with 15 ppm formic acid (experiment FR8).

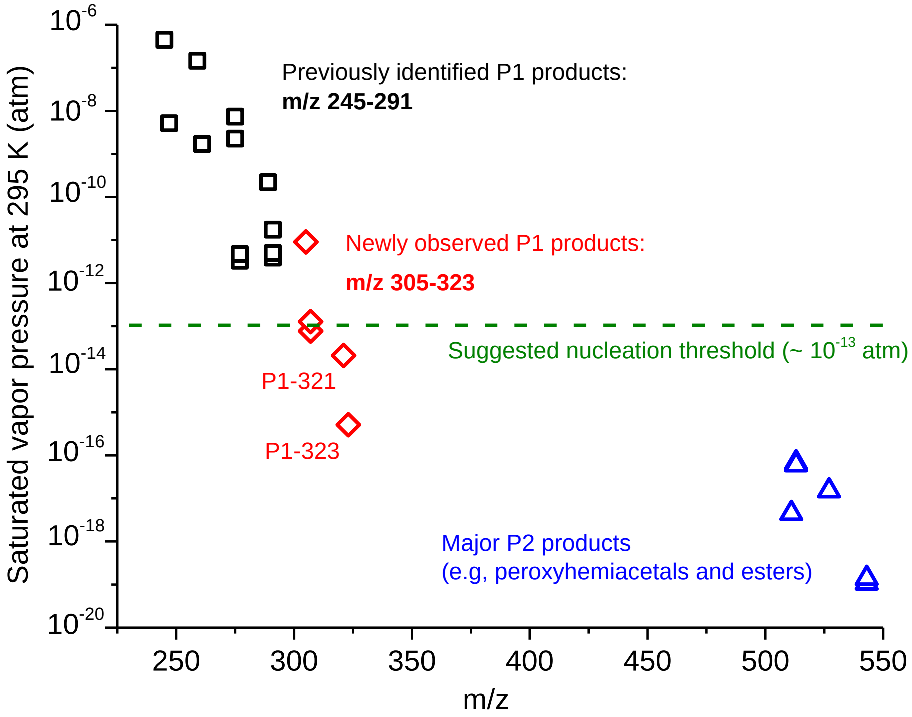

Figure 13 Saturated vapor pressures of typical P1 and P2 products in α-cedrene SOA estimated by taking the average of the predictions from SIMPOL.1 and EVAPORATION. The dashed line indicates the upper limit of saturated organic vapor pressure for nucleation.